sustainability

MDPI

Article

Scale Dependence and Nonlinear Effects of Urban Functional Zone Form on Carbon Emission Intensity: Evidence from Yangtze River Delta Agglomeration

Wanyi Xu [1], Mingzhen Wei [1], Minghao Zuo [2] and Junnan Liu [2,*]

[1] College of Landscape Architecture, Northeast Forestry University, Harbin 150040, China; x.wanyi@nefu.edu.cn (W.X.); 2020224209@nefu.edu.cn (M.W.)
[2] School of Architecture, Tianjin University, Tianjin 300072, China; mayozuo0304@tju.edu.cn
* Correspondence: liujunnan_032@tju.edu.cn

Abstract

Urban functional zones (UFZ) serve as fundamental units of human activity, and their spatial configurations significantly influence urban carbon emissions. However, current research often overlooks the heterogeneity of UFZ forms and the complex, multi-scale relationships underlying their impact on emissions. To address this gap, this study investigates the Yangtze River Delta (YRD) urban agglomeration by delineating UFZ from the dual perspectives of block function and form. By integrating multi-scale spatial analysis with explainable machine learning, this study establishes a morphological indicator system covering three dimensions: density, morphology, and structure. The results reveal a pronounced scale dependency in the effects of UFZ form on carbon emission intensity (CEI), with optimal analytical scales identified at 14 km for density, 5 km for morphology, and 7 km for structure. Notably, variations within these dimensions lead to distinct patterns of impact intensity, even within the same functional category. Furthermore, most indicators exhibit nonlinear, threshold-dependent effects on CEI. These findings provide actionable guidance for fine-grained urban planning and carbon mitigation strategies.

Keywords: urban form; urban functional zones; scale effect; carbon emission intensity; nonlinear effect

1. Introduction

Global climate change, driven by rising concentrations of greenhouse gases, represents one of the most critical challenges facing humanity in the twenty-first century [1]. Among these gases, carbon dioxide emissions constitute the principal driver of climate change [2–4]. As the most irreversible and fastest-growing form of land use dominated by human activities [5], cities account for more than 70% of global energy-related carbon dioxide emissions [6]. This highlights the pivotal role of cities and their substantial potential for carbon mitigation. Consequently, many countries have begun to rethink and redesign their planning frameworks, seeking low-carbon development pathways through adjustments to urban form, spatial layout, and stages of urban development stages [7].

In particular, developing countries are experiencing rapid urbanization and escalating energy demand, which are reshaping global energy consumption patterns and making research on urban form increasingly urgent. Against this backdrop, China, as the largest developing country, has actively assumed international responsibility by committing to

Academic Editor: Ali Bahadori-Jahromi

Received: 2 June 2026
Revised: 27 June 2026
Accepted: 1 July 2026
Published: 9 July 2026

peaking carbon emissions before 2030 and achieving carbon neutrality by 2060 [8], placing green transition at the center of its long-term national strategy. Nevertheless, China continues to face significant challenges, including a relatively short transition period between carbon peaking and carbon neutrality, a fossil-fuel-dominated energy consumption structure, and the prominent role of traditional industrial manufacturing in its economy [9], These challenges underscore the practical importance of achieving the "dual-carbon" goals and provide valuable experience for other developing countries.

Urban form constitutes an integral component of the spatial configuration of human activities [10], shaping urban growth and expansion [11], and consequently influencing carbon dioxide emissions. Notably, a growing body of literature has demonstrated the critical role of urban form in determining carbon emissions [12–14]. For example, studies by Shi et al. and Fang et al. [15,16] reported similar conclusions, indicating that compact development strategies reduce carbon dioxide emissions, whereas urban complexity and sprawl tend to increase them. However, most existing studies utilize total carbon emissions as the dependent variable, which obscures the coordinated relationship between economic activities and carbon outputs. This approach fails to adequately incorporate carbon efficiency, thereby overlooking carbon emission intensity (CEI)—an indicator that better reflects resource utilization efficiency and carbon mitigation potential [17–19]. Furthermore, cities have often been treated as homogeneous entities without differentiation by functional zones, neglecting substantial differences among zones in terms of transportation demand and building energy consumption [20,21]. As a result, carbon emission mechanisms remain incompletely understood, limiting the assessment of the true impact of urban form on CEI. Moreover, findings derived from analyses at the aggregate city scale often have limited practical applicability. For instance, although many studies have shown that compact cities can reduce per capita carbon emissions, compact development may also generate negative externalities such as traffic congestion, localized pollution, and adverse health effects [22]. As a fundamental planning unit, urban functional zones (UFZ) represent the spatial organization of human activities within specific areas [23]. Focusing on UFZ enables the formulation of planning and policy strategies more closely aligned with actual urban functions, supporting finer-grained regulation of carbon emissions and improving the practical relevance of research findings.

Given the limitations of existing studies that treat cities as homogeneous entities, recent research has increasingly shifted its focus toward the differentiated impacts of intra-urban UFZ form on CEI, providing a more fine-grained understanding of how urban form influences carbon emissions. Existing studies can generally be classified into two main categories. The first category, exemplified by Ma et al. [24], emphasizes the attributes of UFZ and examines the heterogeneous effects of different UFZs on carbon emissions within cities. The second category, represented by Huang et al. and Li et al. [25,26], concentrates on finer-scale urban morphology, examining the driving effects of building configurations and green space patterns on carbon emissions. However, both strands of research consider only a single dimension of urban form. The former neglects how variations in UFZ form within UFZs create differentiated thermal environments, resulting in intra-zone differences in energy consumption and associated carbon emissions. The latter overlooks the influence of the functional attributes of different building types on usage scenarios and their important moderating effects on carbon emissions.

As discussed above, existing studies have largely focused on the relationship between urban form and carbon emissions. Although some research has begun to examine the impacts of UFZ form on carbon emissions, three critical gaps remain. First, prior studies have insufficiently emphasized the role of UFZ form in shaping carbon emissions, and difficulties in acquiring large-scale UFZ attributes have resulted in limited analytical precision and an insufficient understanding of how UFZ form influences CEI, particularly with respect to interactions among different UFZ types [27]. Second, while scale sensitivity has been addressed in some studies, most have concentrated on identifying an optimal analytical scale, without further addressing the modifiable areal unit problem (MAUP) [28]. Finally, although previous studies have devoted considerable effort to investigating the mechanisms through which UFZ form affects CEI, they have largely overlooked the differentiated impacts of UFZ form indicators among UFZ with identical functional attributes, thereby limiting their practical applicability.

Based on these research gaps, this study aims to address the following two key questions: (1) How do the effects of UFZ form indicators on CEI vary across areal units at different spatial scales? (2) What nonlinear patterns do UFZ form indicators exhibit in their effects on CEI across different UFZ?

2. Literature Review

2.1. UFZ Form Indicators

Urban form generally refers to the spatial configuration of urban land use [29], representing the spatial organization of human activities [14]. It encompasses land-use patterns and transportation network structures within cities and plays a critical role in shaping land-use efficiency [30], urban compactness [31], and energy performance [32], making it a key element of physical urban planning [33]. Land use and urban road transportation are widely recognized as urban carbon emissions. As urban development has advanced, theories of urban spatial form have continued to evolve, and the indicators used to characterize it have become increasingly diverse. To comprehensively capture urban spatial form, this study developed an urban spatial form assessment framework consisting of three dimensions: density, morphology, and structure.

Density, as a fundamental dimension of urban spatial form, was initially used to describe the concentration of population during the transition from rural to urban areas. As research has evolved, density-related indicators have been progressively expanded to encompass population, buildings, and economic activities, thereby reflecting the overall magnitude or average distribution of urban elements. For example, Huo et al. [34] employed indicators such as urban population, urban building carbon emissions, urban building floor space, and the added value of the tertiary industry to examine the effects of urban spatial form on carbon emissions. In contrast, Liu et al. [35], by contrast, focused primarily on the building perspective and adopted indicators including built-up area, floor area ratio, and site coverage.

The morphology dimension focuses on the external contours of urban land use and modes of spatial expansion, thereby representing the external shape of cities. Its development stemmed from concerns over urban disorderly sprawl and emphasizes improving urban efficiency through more compact development patterns, thereby characterizing the geometric features and expansion trends of urban land use. As noted by Fleischmann et al. [36], urban morphology should incorporate indicators such as building size and footprint, distance, angle, and compactness. An et al. [37] adopted landscape pattern indices, including the largest patch index, number of patches, and edge density, to examine the relationship between urban spatial structure and carbon emissions.

The structure dimension focuses on the complexity and diversity of internal functional layouts within cities, reflecting the logic of internal spatial organization. Inspired by the concepts of New Urbanism and Smart Growth, urban space has increasingly evolved toward mixed, efficient, and compact forms. Accordingly, indicators such as functional mix and land-use diversity have been widely applied to assess the complexity of internal urban spatial relationships and their sustainability. For example, Feng et al. [38] employed land-cover mix and land-nature mix as indicators of the structure dimension.

Although existing studies have proposed preliminary frameworks for selecting urban spatial form indicators, substantial gaps remain that warrant further investigation. Some prior studies emphasize physical urban form and examine its relationships with the ecological environment or carbon emissions, but treat UFZs at a relatively coarse level, often using built-up land or land-use categories as proxies [37]. Other studies focus on urban functional structure, primarily examining the linear effects of planar functional compactness and concentration on carbon emissions [39]. Against this background, this study further refines the existing indicator selection framework. Compared with previous studies, the proposed framework moves beyond the conventional practice of characterizing urban spatial characteristics using built-up areas or land-use categories as proxies and instead captures spatial heterogeneity at the UFZ scale. Moreover, it integrates spatial agglomeration, spatial morphology, and functional organization within a unified analytical framework, providing a multidimensional representation of UFZ form. In addition, the framework incorporates both two-dimensional and three-dimensional morphological indicators, thereby offering a more comprehensive basis for revealing the mechanisms through which UFZ form influences CEI.

2.2. Scale Effects

Scale effects refer to systematic changes in research results that occur with variations in the scale of observation or measurement. Such effects imply that relationships between variables, process behaviors, or physical properties may change substantially with scale, resulting in inconsistent patterns and parameters [40] and ultimately leading to MAUP in many studies.

MAUP was first introduced in 1977 and has since become a major challenge in spatial analysis, as changes in spatial units or levels of aggregation can significantly influence analytical results [28,41]. MAUP generally consists of two components: scale effects and zoning effects. Scale effects arise from changes in spatial scales, whereas zoning effects result from differences in the delineation of spatial units. In this study, UFZ boundaries remained unchanged throughout the analysis, and only spatial scales were varied. Therefore, the influence of zoning effects was largely controlled, and this study focuses primarily on the scale-effect component of MAUP. As demonstrated by numerous studies, the relationships between UFZ form indicators (e.g., compactness and fragmentation) and urban environmental conditions (e.g., carbon and thermal environments) vary with the scale and delineation of areal units [42–44]. Different spatial scales may lead to differences in the significance of their effects, thereby confounding the identification of the mechanisms through which UFZ form influences CEI. Previous studies, such as Ge et al. [42], have examined the scale sensitivity of the effects of UFZ form on carbon emissions. However, these studies primarily identify an overall optimal scale and do not explore how the effects of UFZ form indicators on carbon emissions differ across scales.

In view of these limitations and the potential variability inherent in spatial analysis, further investigation of scale effects remains necessary. Accordingly, this study not only identifies the optimal spatial scales at which UFZ form affects CEI but also examines scale-dependent differences in the influencing factors. These findings provide support for zoned and hierarchical carbon management strategies and facilitate more targeted urban planning and governance.

https://doi.org/10.3390/su18147036

3. Material and Methods

3.1. Material

3.1.1. Study Area

This study focuses on the Yangtze River Delta (YRD) urban agglomeration, a premier economic hub on China's eastern coast. Covering 358,000 km^2 across 41 prefecture-level cities in Shanghai, Jiangsu, Zhejiang, and Anhui, the region has faced escalating carbon emissions driven by rapid urbanization. Understanding the impact of UFZ form on CEI is therefore critical. The YRD serves as an ideal study area because its high development intensity and diverse UFZ types provide a comprehensive sample for analyzing morphological impacts across various developmental stages. Moreover, the region's high economic density concentrates emissions within UFZ, ensuring that even minor morphological optimizations can yield substantial reduction benefits. This representativeness allows the findings to be generalized to other urbanizing regions in China (Figure 1).

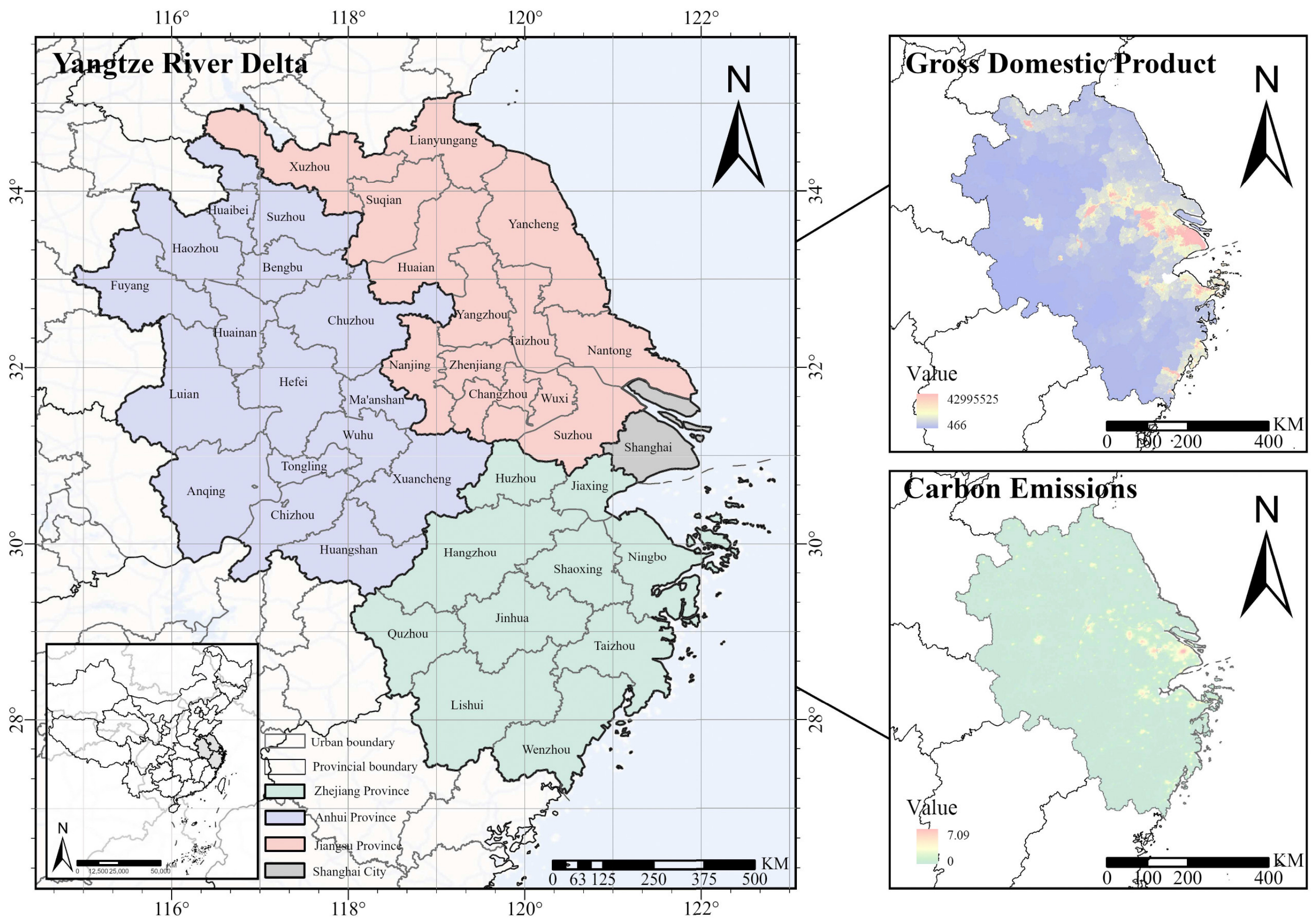

Figure 1. The study area.

3.1.2. Data Sources and Preprocessing

This study analyzes urban carbon emissions using multi-source data, integrating four main data categories: carbon emissions, remote sensing, raster, and vector data. Specifically, it includes data on carbon emissions, land use, Gross Domestic Product (GDP), Normalized Difference Vegetation Index (NDVI), population, roads, buildings, and Point of Interest (POI), as shown in Table 1.

Table 1. Details of the data used for this study.

Category	Name	Time	Source	Resolution
Carbon emissions	ODIAC2024	2023	https://lpdaac.usgs.gov/products/mod11a1v061/ (accessed on 10 January 2026)	1 km
Remote Sensing Data	Annual China Land Cover Dataset	2023	https://doi.org/10.5281/zenodo.8176941	30 m
	Landsat Collection 2 Level-2	2023	https://www.usgs.gov/landsat-missions (accessed on 10 January 2026)	30 m
Grid data	Kilometer Grid Dataset of Spatial Distribution of China's GDP	2020	http://www.resdc.cn/ (accessed on 10 January 2026)	1 km
	VIIRS Nighttime Lights	2023	https://eogdata.mines.edu/products/vnl/ (accessed on 10 January 2026)	500 m
	NDVI Dataset	2023	https://lpdaac.usgs.gov/products/mod13q1v061/ (accessed on 10 January 2026)	30 m
	LandScan	2023	https://landscan.ornl.gov/ (accessed on 10 January 2026)	1 km
Vector data	Vector road map	2023	https://openmaptiles.org/ (accessed on 10 January 2026)	–
	China Multi-Attribute Building	2022–2024	https://doi.org/10.1038/s41597-025-04730-5	0.3–1 m
	POI data	2023	https://lbs.amap.com/api/webservice/guide/api (accessed on 10 January 2026)	–

The data preprocessing is divided into two main parts:

(1) CEI calculation:

Given the limited availability of 2023 1 km × 1 km GDP raster data for the Yangtze River Delta urban agglomeration, this study uses the 2020 1 km × 1 km GDP raster data published by the Institute of Geographic Sciences and Natural Resources Research, Chinese Academy of Sciences. Based on the 2020 GDP raster data and the official GDP statistics of the 41 prefecture-level cities in the Yangtze River Delta for 2020 and 2023, obtained from the official statistical yearbooks and statistical bulletins of the corresponding cities, The ratio of GDP in 2023 to that in 2020 for each city is used as a spatial scaling factor to adjust the 2020 GDP raster, thereby estimating the 2023 GDP raster distribution for the Yangtze River Delta. To further evaluate the validity of this approach, the 2017 GDP raster data were updated to 2020 using city-level GDP growth rates and then compared with the actual 2020 GDP raster data. The results showed a high degree of consistency between the estimated and actual datasets in terms of spatial autocorrelation characteristics and overall spatial patterns, indicating that the approach can effectively preserve the spatial distribution of GDP. In addition, as one of the most economically developed urban agglomerations in China, the Yangtze River Delta urban agglomeration exhibits strong continuity in regional economic activities. Economic growth is largely supported by existing industrial foundations and established urban development patterns, and the spatial distribution of economic activities generally remains relatively stable over short periods. Therefore, applying city-level GDP growth rates as scaling factors to adjust the 2020 GDP raster data provides a reasonable basis for estimating the 2023 GDP raster data. Based on this, the total anthropogenic CO_2 emissions from the 2023 ODIAC dataset are divided by the GDP raster data on a pixel-by-pixel basis to calculate the 2023 CEI for the Yangtze River Delta at a 1 km resolution.

(2) POI Classification:

This study uses the Word2Vec model developed by Google to map POI-related text into word vectors. The model uses neural networks to mine contextual associations of words in large-scale corpora, encoding words into vectors so that semantically similar words are close together in high-dimensional space. Specifically, the Continuous Bag of Words architecture is used, and a separate corpus is created for POI text. The context window is set to 5, and 50-dimensional word vectors are trained. Given that POI texts may contain semantic noise arising from naming heterogeneity, abbreviated expressions, and mixed-use functions, a manually labeled dataset consisting of 20,000 samples is constructed to support supervised classification. By incorporating large-scale manual annotations, the model can more effectively learn category-specific semantic characteristics, thereby mitigating the potential impact of semantic noise on POI classification results. Subsequently, the XGBoost algorithm is applied to classify all POIs into six categories: residential, commercial, industrial, transportation, public services, and open space.

3.2. Methodology

3.2.1. Research Process

The methodological framework (Figure 2) outlines the research process for investigating the impact of UFZ form on CEI. The workflow is synthesized into four sequential steps. First, the study area is divided into fine-scale UFZs using the integrated dataset. Second, form indicators are calculated across three dimensions—density, morphology, and structure—with CEI defined as the dependent variable. A suite of control variables is also established, incorporating socioeconomic factors and micro-scale urban form elements. Third, a multi-scale analysis across 1–15 km grid sizes is conducted; specifically, an XGBoost model combined with SHapley Additive exPlanations (SHAP) is employed to identify the optimal scale by analyzing the effects of principal components derived from principal component analysis (PCA) on CEI. Fourth, XGBoost regression is performed using the original indicators at the three identified optimal scales. By ranking feature contributions and analyzing the response trends of SHAP values to specific indicator variations, the underlying mechanisms through which UFZ form influences CEI are revealed.

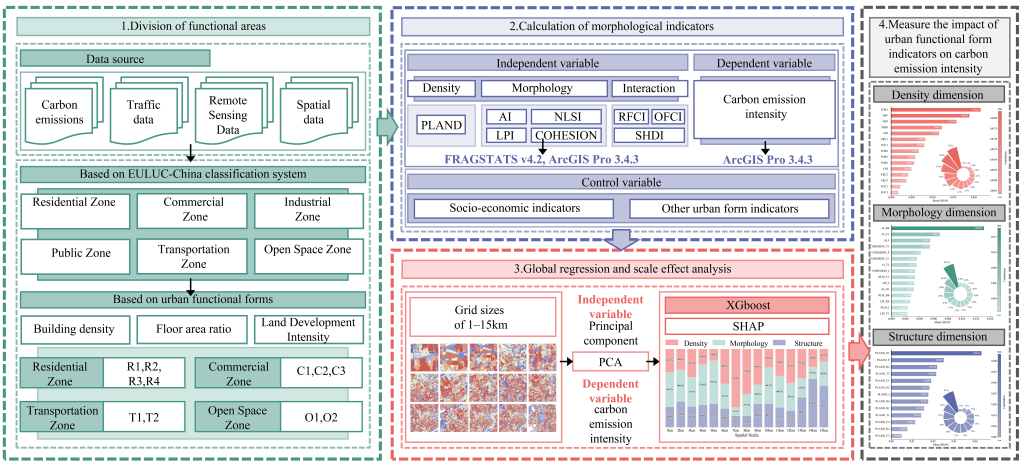

Figure 2. Methodological framework of this study.

3.2.2. Delimitation of UFZ Types

The classification of urban internal functions was conducted in two stages. First, based on the Essential Urban Land Use Categories system for China [45], UFZ were categorized into six primary classes. Notably, open space was designated as a distinct first-level category due to its significant role in regulating urban carbon sequestration and emissions. Second, these categories were further refined based on urban morphology, resulting in thirteen sub-types of functional blocks. This two-tier classification framework aims to facilitate a fine-grained analysis of the heterogeneous impacts of UFZ forms on CEI, as detailed in Table 2.

Table 2. Delimitation of UFZ.

Primary Function Category	Secondary Functional Category
Residential Zone, RZ	High-density mid- and low-rise residential Zone, R1Z Low-density mid- and high-rise residential Zone, R2Z High-density mid- and high-rise residential Zone, R3Z Low-density mid- and low-rise residential Zone, R4Z
Commercial Zone, CZ	Other Commercial Zone, C1Z Individual Commercial Zone, C2Z High-level Commercial Zone, C3Z
Industrial Zone, IZ	Industrial Zone, IZ
Public Zone, PZ	Public Zone, PZ
Transportation Zone, TZ	Transportation road Zone, T1Z Transportation facilities Zone, T2Z
Open Space Zone, OZ	Open green space Zone, O1Z Open square Space Zone, O2Z

This study first calculated Urban Development Intensity (UDI) using a 1 km moving window based on impervious surface data and extracted urban areas using a threshold of UDI > 50% [46]. Subsequently, urban clusters were delineated using the City Clustering Algorithm [47]. For urban core areas, the Simple Non-Iterative Clustering algorithm was employed for superpixel segmentation, and block units were delineated by integrating road, railway, and waterbody data. Based on these units, a total of 68 indicators were derived from remote sensing imagery, POI, population distribution, nighttime light, and building vector data, and an XGBoost classifier was applied to classify UFZs. Finally, the classification results were validated using accuracy assessment metrics.

Based on the identified primary functional categories, a rule-based subdivision approach was further applied to RZs, CZs, and OZs according to their physical form characteristics. RZs were classified into R1Z, R2Z, R3Z, and R4Z according to building density and height. CZs were subdivided into C1Z, C2Z, and C3Z based on building height and maximum building footprint area. OZs were classified into O1Z and O2Z using mean NDVI values. This hierarchical subdivision enables a finer representation of intra-zonal form heterogeneity for subsequent CEI analysis.

3.2.3. CEI

CEI is an important indicator for measuring carbon emissions per unit of economic output and can effectively reflect regional carbon efficiency [48]. Unlike total emissions, CEI normalizes carbon emissions using gridded GDP data, thereby capturing the spatial variation in carbon emissions relative to economic activity. In this study, CEI was defined as the ratio of total CO_2 emissions to actual GDP at the grid level and was calculated as follows:

$$CEI_i = \frac{C_i}{GDP_i} \tag{1}$$

where CEI_i denotes the carbon emission intensity of grid i, C_i represents the carbon emissions, and GDP_i denotes the gross domestic product of grid i.

3.2.4. Measurement of UFZ Form Indicators

Following a comprehensive review of factors influencing CEI, three core dimensions—density, morphology, and structure—are adopted to characterize UFZ form. The density dimension is represented by Percentage of Landscape (PLAND). The morphology dimension includes four landscape pattern indices: Normalized Landscape Shape Index (NLSI), Aggregation Index (AI), Largest Patch Index (LPI), and Patch Cohesion Index (COHESION). These indicators and their derived metrics are calculated using FRAGSTATS v4.2. For the structure dimension, this study builds upon the Functional Compactness Index (FCI) proposed by Lan et al. and further introduces the Residential Functional Compactness Index (RFCI) and Open Space Functional Compactness Index (OFCI) to account for the spatial relationships between OZ and other UFZs, as well as linkages between urban micro-scale form and human activities [27,49]. Shannon's Diversity Index (SHDI) is additionally incorporated to capture functional diversity [50]. Landscape pattern indices are computed using FRAGSTATS, while RFCI, OFCI, and their 16 derived metrics are generated in ArcGIS Pro 3.4.3. In total, 84 indicators are selected as explanatory variables for CEI, as summarized in Table 3.

Table 3. Description of indicators and calculation formula.

Components	Indicators	Abbr.	Formula	Descriptions
Density	Percentage of Landscape	$PLAND_X$	$\frac{\sum a_{ix}}{A} \times 100$	Percentage of the area of a given UFZ type relative to the total patch area.
Morphology	The largest patch index	LPI_X	$\frac{max(a_{ij})}{A} \times 100$	Percentage of the largest patch area of a given UFZ type relative to the total patch area.
	Normalized Landscape Shape Index	$NLSI_X$	$\frac{LSI - LSI_{min}}{LSI_{min} - LSI_{min}}$	Normalized measure of patch edge complexity within a UFZ.
	Aggregation Index	AI_X	$\left[\frac{g_{ii}}{max \rightarrow g_{ii}}\right]$	Degree of aggregation of patches of the same type within a UFZ.
	Patch Cohesion Index	$COHESION\ I_X$	$\left[1-\left(\frac{\sum_i p_i}{\sum_i \sqrt{a_i}}\right)/\left(1-\frac{1}{\sqrt{n}}\right)\right]\times 100$	Connectivity and cohesion of patches within a UFZ.
Structure	Residential Functional Compactness Index	$RFCI$	$\sum F_{RX}$	Composite indicator quantifying UFZ compactness, where F_{RX} denotes the spatial interaction between residential human activity intensity and that of another zone.
		F_{RX}	$\frac{1}{MN}\sum_{i\in\varphi_i}\sum_{j\in\varphi_j}\frac{1}{c}\frac{R_i X_j}{d^2(i,j)}$	
	Open space Functional Compactness Index	$OFCI$	$\sum F_{OX}$	Degree of functional coupling between urban green and open spaces and other UFZ, where F_{OX} denotes the spatial interaction between ecosystem service intensity of green and open spaces and human activity intensity in another zone.
		F_{OX}	$\frac{1}{MN}\sum_{i\in\varphi_i}\sum_{j\in\varphi_j}\frac{1}{c}$	
	Shannon's Diversity Index	$SHDI$	$-\sum_i (p_i \ln p_i)$	Diversity of different patch types within a UFZ.

Note: X = R1, R2, R3, R4, C1, C2, C3, P, I, T1, T2, O1, O2. In RFCI and OFCI, X denotes human activity intensity of UFZs, excluding the target UFZ and TZs.

In addition, to control for other factors that may influence CEI, a total of eight control variables were incorporated into the model, covering both socioeconomic factors and micro-scale urban form characteristics. At the socioeconomic level, five indicators were included as control variables, namely total population, total GDP, GDP per capita, green patent authorizations, and the mean kernel density of high-tech enterprises, based on STIRPAT theory [51]. At the micro-scale urban form level, three indicators, including building density, floor area ratio, and land development intensity, were introduced as control variables to isolate the effects of other morphological factors on CEI, thereby retaining UFZ form as the primary focus of analysis.

3.2.5. Scale Effect Analysis

To identify the optimal spatial scales at which UFZ form influences CEI, fishnet grids ranging from 1 to 15 km were generated. The minimum scale was set to 1 km because both the GDP and carbon emission datasets used to calculate CEI have a spatial resolution of

1 km, which makes finer-scale analysis unreliable and impractical. The maximum scale of 15 km was determined with reference to previous studies on UFZ morphology and because it is sufficiently large to encompass most built-up areas of some small and medium-sized cities, thereby capturing broader urban spatial organization patterns [42]. Using these multi-scale grids, XGBoost regression models were fitted separately at each scale. XGBoost is an efficient gradient boosting decision tree algorithm widely applied in prediction tasks, which improves performance by integrating multiple decision trees into a unified ensemble framework [52,53]. In addition, XGBoost does not require predefined functional relationships between independent and dependent variables and can automatically capture complex nonlinear relationships and interaction effects. Furthermore, the SHAP method can be integrated to quantify the contributions of indicators with different scales and characteristics to model outputs, thereby enhancing the interpretability of the results. Given that 82 UFZ form indicators were included in this study and that high collinearity may hinder the identification of independent effects, PCA was employed for dimensionality reduction and feature extraction [54]. PCA was employed solely to reduce multicollinearity among indicators within each morphological dimension and to generate integrated representations for optimal-scale identification. The extracted principal components were not used for subsequent mechanism interpretation, as all final analyses were conducted using the original morphological indicators. To verify the effectiveness of PCA for dimensionality reduction, the newly generated variables were evaluated using the Variance Inflation Factor (VIF) after data processing. Following the VIF < 10 criterion commonly adopted in urban morphology studies [55,56], the level of multicollinearity among variables was assessed. In addition, given that machine learning models are generally less sensitive to multicollinearity, moderate correlations among explanatory variables are unlikely to substantially affect model performance.

The specific procedures for global regression and scale effect analysis are as follows: First, the study area is partitioned into grids with resolutions ranging from 1 km to 15 km in size. For each scale, the UFZ raster dataset was partitioned using the corresponding fishnet grid, and landscape pattern indicators were calculated in FRAGSTATS. FCI indicators were calculated based on the spatial correspondence between 1 km grids and larger-scale grid units. The resulting indicator datasets were standardized and subsequently subjected to principal component extraction to reduce multicollinearity among indicators. Second, the principal components obtained from PCA are used as explanatory variables, with CEI as the dependent variable and socioeconomic and other urban form indicators as control variables, and XGBoost regression is conducted separately at each grid scale from 1 km to 15 km. Finally, to enhance interpretability, optimal scales for analyzing UFZ form are identified based on the mean absolute |SHAP| values and the scale-dependent contribution shares of principal components across the three dimensions.

3.2.6. Nonlinear Impact Characteristics

To further examine the nonlinear effects of UFZ form indicators across the density, morphology, and structure dimensions on CEI, regression analyses were performed at the identified optimal scales using the original indicators corresponding to each principal component within the XGBoost model. First, indicators were ranked based on mean absolute SHAP values, and the top twelve contributors were selected. Second, for each significant indicator, nonlinear response curves were derived by fitting locally weighted scatterplot smoothing (LOWESS) to plots of indicator values versus SHAP values, with 95% confidence intervals estimated using the bootstrap method. This procedure enables quantification of each feature's contribution to model predictions and systematically evaluates the importance and directional effects of UFZ form indicators across different dimensions on CEI at the optimal spatial scale.

4. Results

4.1. Identification of UFZ

Based on road network and POI data, the study area was ultimately classified into 13 UFZ types. In the first-level functional zoning, the XGBoost classifier exhibited good performance on the test set, achieving an overall accuracy of 0.85 and a Kappa coefficient of 0.80, indicating its effectiveness in distinguishing different UFZ. Among all zones, residential UFZ—including high-density high-rise, high-density mid–low-rise, low-density high-rise, and low-density mid–low-rise residential areas—were the most widespread, accounting for 33.97% of the total area. Industrial UFZ ranked second, covering 25.29%. OZ, including green open spaces and open plazas, accounted for 16.26%, while transportation UFZ, comprising transport corridors and facilities, covered 11.80%. Other UFZ, such as public service and CZs, occupied relatively smaller areas, accounting for 7.86% and 4.82%, respectively. The spatial distribution and composition of these UFZ are illustrated in Figure 3.

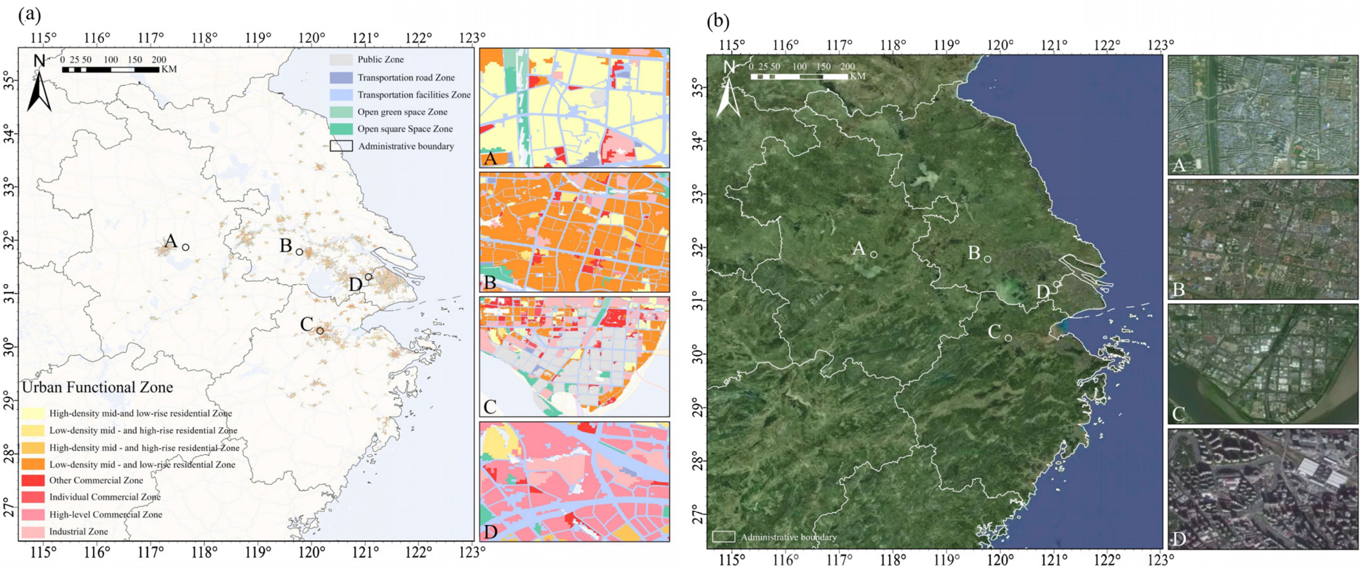

Figure 3. Illustration of (**a**) UFZ classification results and (**b**) remote sensing image.

The secondary subdivision was generated using a morphology-based rule-based method. Therefore, its reliability was evaluated through visual comparison with 2023 high-resolution satellite imagery. Specifically, Zone A corresponds to high-density mid–low-rise residential areas, Zone B to low-density mid–low-rise residential areas, Zone C to industrial zones, and Zone D to high-rise commercial zones. The results show a high degree of consistency between the identified UFZ types and the actual urban morphological characteristics observed in the satellite imagery. Clear differences in building density, building height, and vegetation coverage are evident among the secondary UFZ categories, indicating that the subdivision effectively captures the morphological heterogeneity of different UFZ subtypes.

4.2. Characteristics of CEI

Based on the spatial autocorrelation analysis of CEI in the YRD in 2023 (Figure 4), a clear and significant pattern of spatial clustering is evident. At the county level, Low–Low clusters are the most prevalent and are mainly distributed contiguously along the eastern

https://doi.org/10.3390/su18147036

coastal areas of the YRD. High–High clusters are the second most common, primarily located in Anqing in the west and Bengbu in the north, where industrial transfers from surrounding economically developed regions have occurred and where traditional manufacturing and heavy industries still account for a large share of the industrial structure. Low–High outliers are mainly distributed around High–High clusters and exhibit transitional characteristics, with limited industrial activity, relatively low GDP, and relatively low industrial emissions. High–Low outliers are the least common and are sporadically distributed in Nanjing and Shanghai, where surrounding counties mainly host low-emission, high value-added industries, while these specific counties concentrate high-emission and energy-intensive production functions within cities.

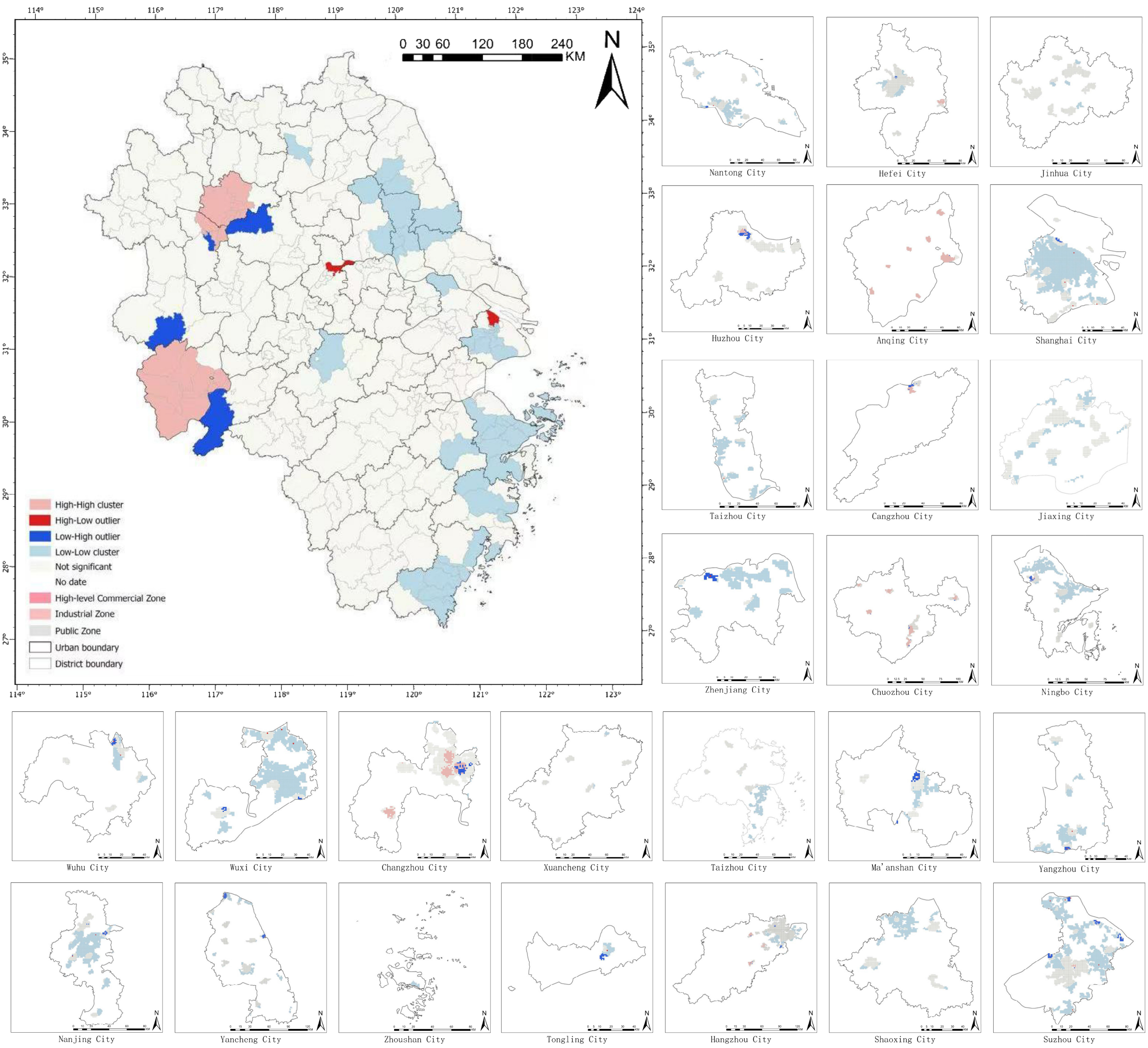

Figure 4. Spatial clustering of CEI.

At the intra-urban scale, the study region comprises 41 cities, of which 15 lack sufficiently developed built-up areas; therefore, the remaining 26 cities were retained for analysis. The results show that the spatial distribution of CEI in the YRD departs from the contiguous clustering pattern observed at the macro scale and instead exhibits a pronounced core–periphery structure. Grid-level CEI displays a patchy spatial pattern, corresponding to internal UFZ configurations, and demonstrates greater fragmentation and functional mixing than that observed at the regional scale. Specifically, urban core areas are predominantly characterized by Low–Low clusters, whereas High–High clusters are more likely to occur in peripheral zones, suburban areas, or subordinate counties. This pattern reflects the concentration of modern service-oriented industries, such as finance and innovation-driven sectors, in high-cost central areas, where energy consumption per unit GDP is relatively low. In contrast, energy-intensive manufacturing activities tend to relocate toward urban fringes and suburban areas to reduce production costs. These findings highlight the decisive role of intra-urban functional differentiation in shaping the spatial heterogeneity of CEI.

Owing to the substantial disparities in economic scale among cities within the YRD, CEI is adopted instead of total carbon emissions to minimize the influence of differences in economic and population size, thereby ensuring comparability across cities with different development levels. The results indicate that CEI more effectively reflects variations in industrial structure and the level of green technological development in economic activities, clearly distinguishing the technological gradients and industrial hierarchies between core and peripheral areas of the YRD.

4.3. Scale-Dependent Characteristics

The suitability of the data was first examined prior to factor extraction. The results of Bartlett's test of sphericity showed that all variables were significant at the 0.01 level, suggesting that the sample correlation matrix deviates from an identity matrix and that meaningful correlations exist among variables. These results confirm the appropriateness of conducting factor analysis. Based on this, PCA was employed to perform dimensionality reduction and feature extraction on the original indicator system. A total of 8, 12, and 9 principal components were extracted from the density, morphology, and structure dimensions, respectively. The cumulative variance explained by the retained components was recorded at different spatial scales. Subsequently, VIF tests were conducted on all extracted principal components to assess multicollinearity. The results are reported in Table 4.

Table 4. Results of PCA and VIF Tests.

Scale (km)	Cumulative Variance Contribution Rate			Maximum VIF Value
	Density	Morphology	Structure	
1	73.78%	70.02%	69.12%	6.01
2	75.71%	70.11%	71.08%	4.74
3	75.78%	70.26%	72.58%	4.25
4	78.40%	71.74%	73.13%	3.89
5	80.19%	72.17%	70.99%	3.62
6	77.13%	71.61%	76.12%	3.69
7	78.66%	72.64%	74.87%	3.49
8	80.37%	73.38%	77.08%	3.96
9	79.97%	73.52%	77.42%	3.98
10	80.63%	73.44%	74.58%	3.3
11	81.99%	73.02%	75.66%	5.26
12	82.12%	74.98%	77.97%	4.2
13	80.54%	74.60%	81.41%	5.24
14	83.08%	75.57%	83.14%	6.26
15	80.27%	75.03%	79.64%	5.36

Based on the table, the three indicator groups exhibit consistently high cumulative variance explained across spatial scales, indicating that the principal components extracted by PCA retain most of the information contained in the original variables, and that the dimensionality reduction is both reasonable and effective. Moreover, the degree of information concentration for the density, morphology, and structure indicators varies across scales, underscoring the necessity of a multi-scale analytical framework.

Based on the XGBoost–SHAP results, the three UFZ form dimensions exhibit pronounced scale dependence and nonlinear behavior in their explanatory shares of CEI. As the analytical scale increases from 1 km to 15 km, the relative contributions of each dimension undergo clear stage-wise reconfiguration (Figure 5), forming a dynamic pattern of alternating dominance across scales. This indicates that the impact of UFZ form on CEI is not driven by a single factor, but arises from the joint effects of multiple spatial dimensions and their interactions.

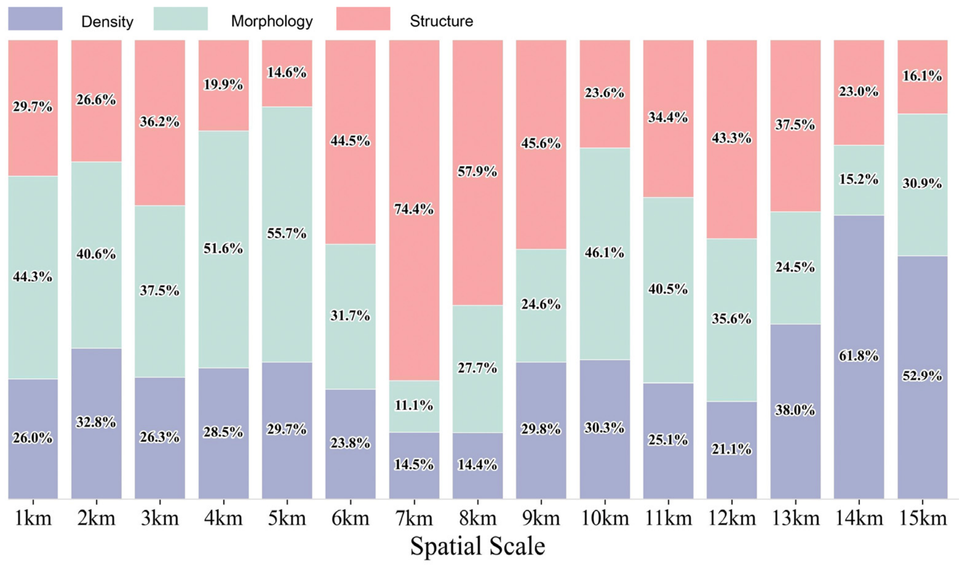

Figure 5. Stacked bar chart of contribution percentages.

Specifically, the contribution of the density dimension is relatively constrained at finer scales but exhibits a stable-then-rising trend as the spatial extent expands, peaking at 61.8% at the 14 km scale. This pattern underscores a pronounced macro-scale accumulation effect, whereby the concentration of high development intensity and population activity over large areas collectively amplifies regional energy demand and CEI. In contrast, the morphology dimension follows a U-shaped trajectory, reaching its maximum contribution of 55.7% at the 5 km scale. This suggests that at localized spatial scales, morphological attributes—such as patch geometric complexity and aggregation—play a direct role in shaping local spatial organization. These characteristics influence micro-level travel behavior and the efficiency of energy use allocation. As the spatial scale increases, however, the explanatory power of localized morphological traits gradually weakens relative to broader spatial processes. The structure dimension exhibits an inverted U-shaped pattern and becomes the dominant contributor at the 7 km scale, peaking at 74.4%. At this intermediate scale, the spatial configuration among distinct urban functional units is most clearly expressed, and the degree of functional coordination or separation exerts a strong influence on commuting distances and energy consumption patterns. At smaller or larger scales, the explanatory power of the structural dimension declines, indicating that its effects are primarily concentrated within a medium spatial range that integrates local functional organization with overall urban connectivity.

Therefore, based on the above scale-effect analysis, 14 km, 5 km, and 7 km are selected as the optimal analytical scales for the density, morphology, and structure dimensions, respectively. At these scales, the original indicators of each dimension are further examined in relation to CEI, enabling more targeted and interpretable insights into their effects.

4.4. Nonlinear Patterns of UFZ Form on CEI

In this study, the effects of original UFZ form indicators on CEI were examined across the three dimensions of density, morphology, and structure. SHAP was employed to interpret the XGBoost regression results, with SHAP summary plots used to rank indicator importance within each dimension and SHAP dependence plots applied to visualize the nonlinear response relationships between indicators and CEI. The results reveal pronounced heterogeneity in the dominant factors across different form dimensions, indicating substantial differences in their explanatory power. Moreover, the relationships between UFZ form indicators and CEI exhibit clear nonlinear and threshold effects.

As shown in the SHAP summary plot in Figure 6, the density dimension captures the contributions of area proportions of different UFZ types at the optimal scale. Indicators related to OZ and PZ exhibit relatively high importance in model interpretation. Notably, the importance of R2Z is substantially higher than that of high-density residential types (R1Z and R3Z), indicating that, even under comparable land-use proportions, different residential typologies reflecting distinct spatial organization exert markedly different influences on the CEI.

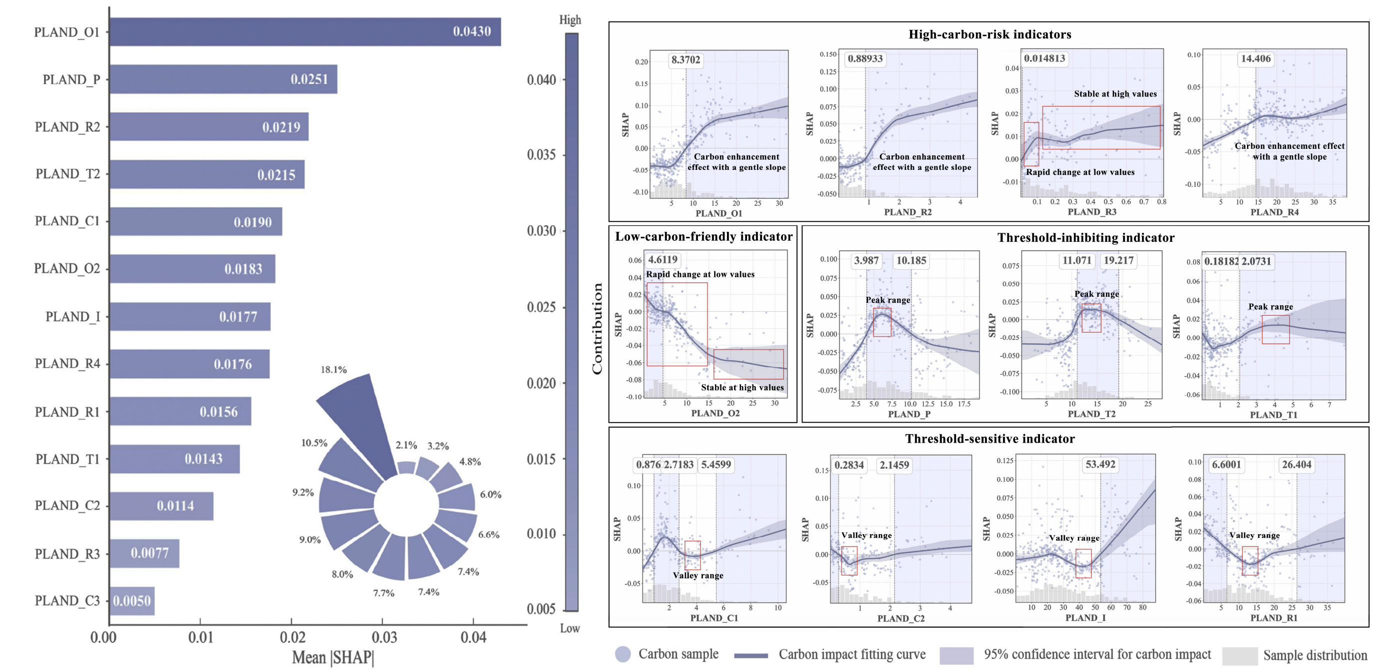

Figure 6. Effects of density-related UFZ form indicators on CEI.

Based on the SHAP dependence plots of individual indicators, the major contributors to CEI within the density dimension can be classified into four response types. The first group represents high-carbon-risk indicators, including PLAND_O1, PLAND_R2, PLAND_R3, and PLAND_R4. Among them, PLAND_O1 and PLAND_R2 exhibit carbon-reducing effects at low values, but their marginal effects gradually diminish. Once the indicator values exceed specific thresholds, their effects reverse from carbon reduction to carbon promotion, after which the response curves gradually level off, indicating diminishing marginal effects. PLAND_R3 and PLAND_R4 both show an overall increasing trend with increasing indicator values, but their response patterns differ substantially. PLAND_R3 consistently exhibits a carbon-increasing effect, with a particularly strong marginal effect at low values. In contrast, PLAND_R4 reduces CEI at low and medium values, whereas its mitigation effect gradually weakens and eventually shifts to a carbon-increasing effect after the threshold is exceeded. The second group consists of low-carbon-friendly indicators, represented by PLAND_O2. Although O1Z and O2Z both belong to open space land uses, they exhibit markedly different response patterns. Once PLAND_O2 exceeds the threshold of 4.6119, it consistently produces a stable carbon-reducing effect. The third group comprises threshold-inhibiting indicators, including PLAND_P, PLAND_T2, and PLAND_T1. All three exhibit pronounced inverted U-shaped relationships with CEI. Their carbon-promoting effects peak near specific threshold values and then gradually reverse into carbon-reducing effects as the indicator values continue to increase. The fourth group includes threshold-sensitive indicators, namely PLAND_C1, PLAND_C2, PLAND_I, and PLAND_R1. These indicators all exhibit distinct troughs corresponding to the minimum CEI. Around these thresholds, land-use efficiency, population concentration, and energy intensity reach an optimal balance, thereby maximizing the low-carbon scale effect.

As shown in the SHAP summary plot in Figure 7, within the morphology dimension, the AI and COHESION exhibit substantially higher importance than other form indicators. Among the various UFZ form indicators, those associated with RZ and C1Z exhibit relatively stronger influences on CEI.

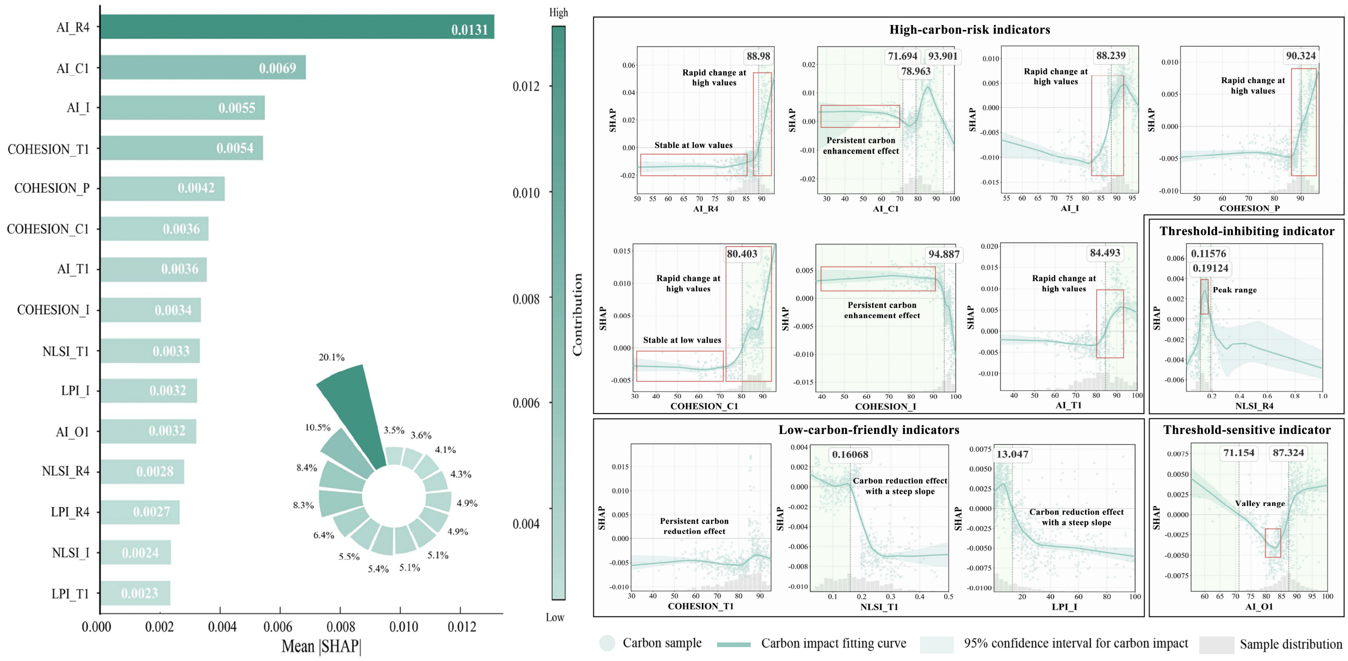

Figure 7. Effects of morphology-related UFZ form indicators on CEI.

Specifically, the first group consists of high-carbon-risk indicators, including AI_R4, AI_C1, AI_I, COHESION_P, COHESION_C1, COHESION_I, and AI_T1. Among them, AI_R4, COHESION_P, and COHESION_C1 exhibit relatively stable SHAP values at low and medium levels, indicating consistent carbon-reducing effects as increasing aggregation or connectivity improves spatial organization and resource allocation efficiency. However, once the indicator values approach high-value thresholds, their SHAP values increase sharply and become positive, indicating a rapid transition to carbon-increasing effects. AI_I and AI_T1 show similar response patterns at low and medium values but exhibit an asymmetric U-shaped trend at higher values, with SHAP values first increasing and then declining. AI_C1 and COHESION_I generally exhibit stable carbon-increasing effects across most value ranges. Notably, AI_C1 crosses a second threshold at high values, after which its SHAP value declines and the indicator regains a carbon-reducing effect, potentially reflecting the scale effects generated by commercial agglomeration. The second group represents low-carbon-friendly indicators, including COHESION_T1, NLSI_T1, and LPI_I. COHESION_T1 exhibits a stable and persistent carbon-reducing effect across its value range.

By contrast, NLSI_T1 and LPI_I initially show carbon-increasing effects at low values, but these rapidly reverse into carbon-reducing effects as the indicator values increase, after which the response curves gradually level off. The third group comprises threshold-inhibiting indicators, represented by NLSI_R4. This indicator exhibits a pronounced marginal effect at low values and follows a nonlinear response pattern in which CEI initially increases and then decreases. Its carbon-promoting effect reaches a peak at approximately 0.15, after which it gradually weakens and stabilizes into a sustained carbon-reducing effect when the indicator value approaches 0.40. The fourth group consists of threshold-sensitive indicators, represented by AI_O1. This indicator exhibits a pronounced U-shaped response pattern, indicating the existence of an optimal threshold range.

As shown in the SHAP summary plot in Figure 8, within the structure dimension, F_{OX} exhibits relatively higher importance than other form indicators, accounting for 55% of the total contribution, while FRX contributes 35.7%. SHDI also ranks among the leading contributors. These results indicate that, although functional mix can partly explain CEI, the combined effects of inter-zonal compactness and functional composition provide stronger explanatory power.

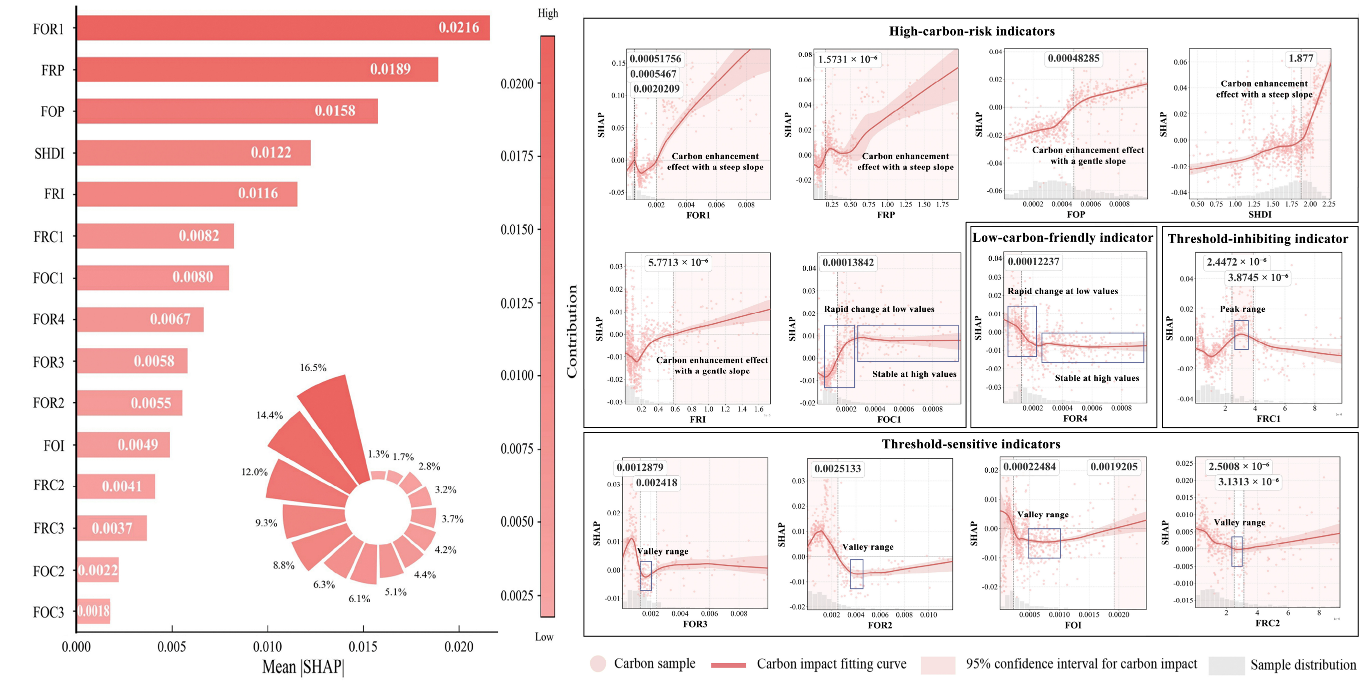

Figure 8. Effects of structure-related UFZ form indicators on CEI.

Specifically, the first group consists of high-carbon-risk indicators, including F_{OR1}, F_{RP}, F_{OP}, SHDI, F_{RI}, and F_{OC1}. These indicators all exhibit carbon-reducing effects at low and medium values, but their effects reverse into persistent carbon-increasing effects after crossing specific thresholds. Among them, F_{OR1}, F_{RP}, and SHDI display steep response curves after the transition, indicating a rapid increase in their carbon-promoting effects. Notably, the response pattern of SHDI suggests that simply increasing functional diversity does not necessarily lead to sustained carbon reduction. By contrast, F_{OP}, F_{RI}, and F_{OC1} exhibit more gradual response curves after the transition, indicating that their carbon-promoting effects increase at a slower rate. The second group represents low-carbon-friendly indicators, represented by F_{OR4}. This indicator initially exhibits a carbon-increasing effect at low values. As the indicator value increases, its carbon-promoting effect gradually weakens and eventually shifts to a stable carbon-reducing effect after the threshold is exceeded. The third group comprises threshold-inhibiting indicators, represented by F_{RC1}.

This indicator exhibits a pronounced inverted U-shaped response pattern. Its carbon-promoting effect reaches a maximum near the peak value, whereas both low and high values are associated with carbon-reducing effects. The fourth group consists of threshold-sensitive indicators, including F_{OR3}, F_{OR2}, F_{OI}, and F_{RC2}. These indicators all exhibit distinct troughs, indicating the existence of optimal threshold ranges at which their carbon-reducing effects are maximized.

5. Discussion

5.1. Scale Effects of UFZ Form on CEI

This study underscores the intrinsic scale dependency in how multi-dimensional UFZ form influences CEI. Our findings are consistent with prior research emphasizing the necessity of multi-scale approaches for assessing the environmental effects of urban spatial configurations, including air pollution and thermal environments [57]. Studies focusing on high-density urban areas indicate that the explanatory power of built-up spatial patterns, quantified using landscape metrics, varies with grid size at finer spatial scales [58]. In contrast, analyses at the city scale reveal that different landscape metrics exhibit distinct scale effects on air pollution when evaluated at coarser spatial resolutions [42,59].

The results further demonstrate that scale effects do not manifest uniformly across different dimensions of UFZ form. By decomposing UFZ form into density, morphology, and structure, this study shows that its effects on CEI are strongly scale-dependent. These effects do not operate in isolation; instead, they interact and evolve dynamically as spatial scale changes. As grid size increases, the contribution of density remains relatively stable at finer scales but exhibits a clear upward trend at larger scales, indicating that density-related effects tend to accumulate and become more pronounced over broader spatial extents. In contrast, the contributions of morphology and structure display distinct nonlinear patterns. Morphological indicators exhibit a U-shaped relationship with scale, reaching their maximum explanatory power at relatively fine spatial resolutions, whereas structural indicators follow an inverted U-shaped pattern and dominate at intermediate scales. These differences reflect heterogeneous spatial mechanisms through which each dimension operates. Specifically, at the density dimension, a 14 km grid effectively captures the cumulative impacts of urban built-up intensity, enabling a more accurate understanding of how large-scale development patterns influence CEI [60]. At the morphology dimension, patch shape, aggregation, and connectivity primarily affect CEI through localized processes [61]. Consequently, at the 5 km grid scale, morphology indicators are better able to characterize neighborhood-level spatial structures, leading to peak explanatory power. At the structure dimension, indicators mainly describe the spatial configuration and diversity of UFZs. At the 7 km scale, the combined arrangement of multiple functional areas is sufficiently represented, allowing functional coordination to exert stronger influences on commuting distances, travel organization, and energy consumption patterns. As a result, structural characteristics demonstrate their greatest explanatory capacity at this intermediate spatial scale.

Overall, our findings extend existing multi-scale analytical frameworks by explicitly revealing the heterogeneous scale responses across different dimensions of UFZ form. This indicates that the impacts of urban form on carbon emissions are jointly shaped by spatial extent and functional organization, rather than being driven by a single dominant scale or a single category of form indicators.

5.2. Impact Characteristics of UFZ Form on CEI

5.2.1. Effects of Density-Related Indicators on CEI

The density dimension reflects how the spatial allocation of UFZs influences CEI. Overall, OZ, PZ, RZ, and TZ are more influential than production-related zones, indicating that the organization of human activities and service provision dominates over production scale in shaping carbon emissions.

OZ configuration plays a significant role in CEI. O1Z is generally associated with increased carbon emissions, likely due to longer travel distances and higher maintenance energy demand for large, concentrated green spaces [62]. In contrast, O2Z consistently exhibits carbon-reducing effects, suggesting that hierarchical open-space systems can better balance ecological benefits and service efficiency. RZ expansion increases CEI through higher building energy use, household electricity demand, heating consumption, and traffic congestion [63]. Among residential subtypes, R2Z shows a stronger effect than R1Z, R3Z, and R4Z, which may result from the combination of low-density layouts and high-rise buildings that jointly increase transport energy use and operational energy demand [64]. Accordingly, controlling low-density high-rise residential expansion and improving jobs–housing balance and transport accessibility is essential. PZ and TZ exhibit nonlinear effects with clear threshold behavior. At moderate levels, expansion intensifies transport activity and increases CEI, whereas at higher levels, both zones shift toward carbon mitigation. This may reflect scale effects in public services and congestion-relief effects of transport infrastructure [65]. Therefore, both land types should be managed within appropriate threshold ranges.

Overall, density effects arise from how land allocation regulates human activity and transport demand. Most UFZs exhibit clear threshold ranges, beyond which either excessive concentration or dispersion weakens carbon mitigation potential.

5.2.2. Effects of Morphology-Related Indicators on CEI

The morphology dimension shows that aggregation and connectivity exert stronger effects on CEI than other structural characteristics, highlighting the importance of spatial organization.

R4Z, C1Z, IZ, and T1Z consistently show a pattern where moderate aggregation reduces CEI, while excessive aggregation increases it. This suggests that efficiency gains from spatial concentration exist only within a limited range, beyond which increased mobility demand, energy consumption, and anthropogenic heat dominate. IZ and T1Z exhibit clearer scale effects. Larger patch size in IZ and higher connectivity in T1Z contribute to reduced CEI, indicating that spatial concentration and network efficiency benefit production and transport systems [66]. Open spaces follow a different mechanism. Moderate clustering improves ecological efficiency, but excessive aggregation reduces service accessibility, while excessive fragmentation weakens ecological continuity. Therefore, planning must balance ecological integrity and accessibility rather than maximizing aggregation alone.

Overall, all UFZ types exhibit clear threshold effects in morphological responses, suggesting that urban form optimization should focus on maintaining key morphological indicators within suitable ranges rather than maximizing single structural properties.

5.2.3. Effects of Structure-Related Indicators on CEI

The structure dimension highlights the importance of spatial linkages among UFZs in shaping CEI, with FOX identified as the most influential factor, followed by FRX and SHDI.

Spatial interactions between OZ and RZ, C1Z, and PZ strongly affect CEI. Most indicators exhibit a clear transition from carbon reduction to carbon increase as coupling intensifies, indicating that excessive spatial interaction increases mobility demand and energy consumption. F_{OR1}, F_{OC1}, F_{OR3}, and F_{OR2} show pronounced threshold behavior around 0.002, suggesting that inter-zone linkage intensity should be carefully controlled below this level. In contrast, FOP exhibits carbon-increasing effects only at relatively high values, reflecting stronger functional complementarity and coordination between PZ and OZ. FOR4 differs from other residential-related indicators by maintaining stable carbon-reducing effects, suggesting that low-density residential areas combined with open space support low-energy activities such as walking and recreation. By contrast, excessive coupling between RZ and PZ at medium to high levels significantly increases CEI, indicating that residential–service integration should be carefully regulated.

It is worth noting that SHDI also exhibits a distinct threshold effect with respect to CEI, contrasting with previous studies that generally reported a persistent carbon-reduction effect of functional diversity. At low to moderate levels, functional diversity improves land-use efficiency and spatial organization efficiency, thereby reducing carbon emissions. Beyond the threshold, however, excessive functional diversity reflects increasingly fragmented and dispersed spatial configurations, which increase transportation demand, energy consumption, and anthropogenic heat emissions. In addition, it may reduce the continuity of blue–green spaces and weaken urban ecological regulation capacity [67]. Together, these mechanisms contribute to a nonlinear shift from carbon mitigation to carbon promotion, resulting in a rapid increase in CEI once the threshold is exceeded.

Overall, structural effects are more complex than those of individual UFZ characteristics. Most indicators exhibit distinct threshold ranges, suggesting that effective carbon mitigation depends on optimizing inter-functional spatial coordination rather than focusing on single land-use attributes.

5.3. Differences in the Effects of UFZ Form on CEI Between Core and Peripheral Cities

Owing to pronounced differences in economic conditions and institutional contexts between core and peripheral cities [68], the relationships between functional land use and CEI vary across different stages of urban development. To further examine the heterogeneous effects of key driving factors at different development stages, cities within the YRD were classified into core and peripheral groups based on their administrative hierarchy. Specifically, core cities include municipalities directly under the central government, provincial capitals, and sub-provincial cities, whereas peripheral cities comprise all remaining prefecture-level cities [69]. On this basis, separate analyses were conducted for core and peripheral cities to compare the differential contributions of UFZ form indicators to CEI across the density, morphology, and structure dimensions.

A comparison of the SHAP summary plots for the density dimension reveals clear contrasts between core and peripheral cities (Figure 9). In core cities, the influence of density-related indicators on CEI appears relatively concentrated, with carbon emission intensity being primarily driven by the area proportion of CZ, in addition to OZ discussed earlier. In contrast, peripheral cities exhibit a much more diversified set of density-related drivers, in which the proportions of RZ, PZ, IZ and TZ play more prominent roles. This finding indicates that the impact of density on CEI is highly contingent on the stage of urban development, underscoring the need for differentiated density regulation strategies between core and peripheral cities, rather than adopting a uniform compact city strategy.

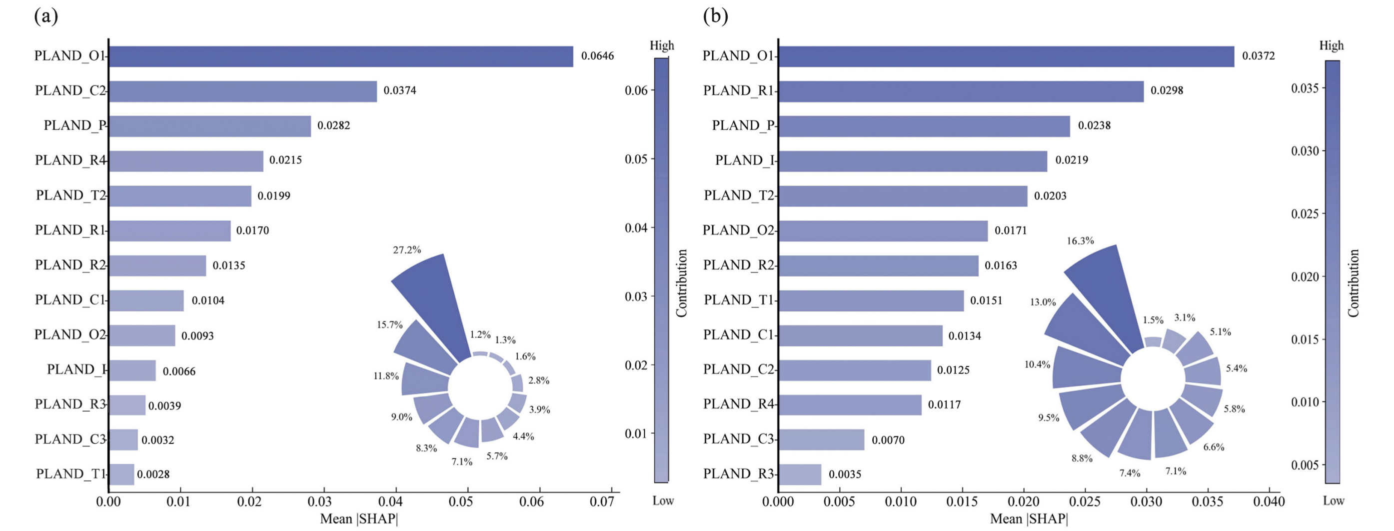

Figure 9. Differences in the contributions of density indicators to CEI between (**a**) core and (**b**) peripheral cities.

Based on the comparison of SHAP summary plots for morphology indicators (Figure 10), the impacts of land-use aggregation and the largest patch index dominate the influence on CEI in core cities, whereas peripheral cities are jointly affected by connectivity, aggregation, fragmentation, and the largest patch index. In core cities, the effects of morphology are primarily driven by the spatial aggregation and patch characteristics of PZ and RZ, with the connectivity of PZ and the aggregation degree of R4Z exhibiting the strongest contributions. By contrast, in peripheral cities, morphology-related effects are more strongly associated with the form characteristics of TZ, RZ, CZ, and IZ, among which TZ connectivity and RZ aggregation emerge as the key driving factors. Overall, the mechanisms through which morphology influences CEI exhibit pronounced stage-dependent differences between core and peripheral cities, underscoring the necessity of adopting differentiated spatial form optimization strategies across urban types.

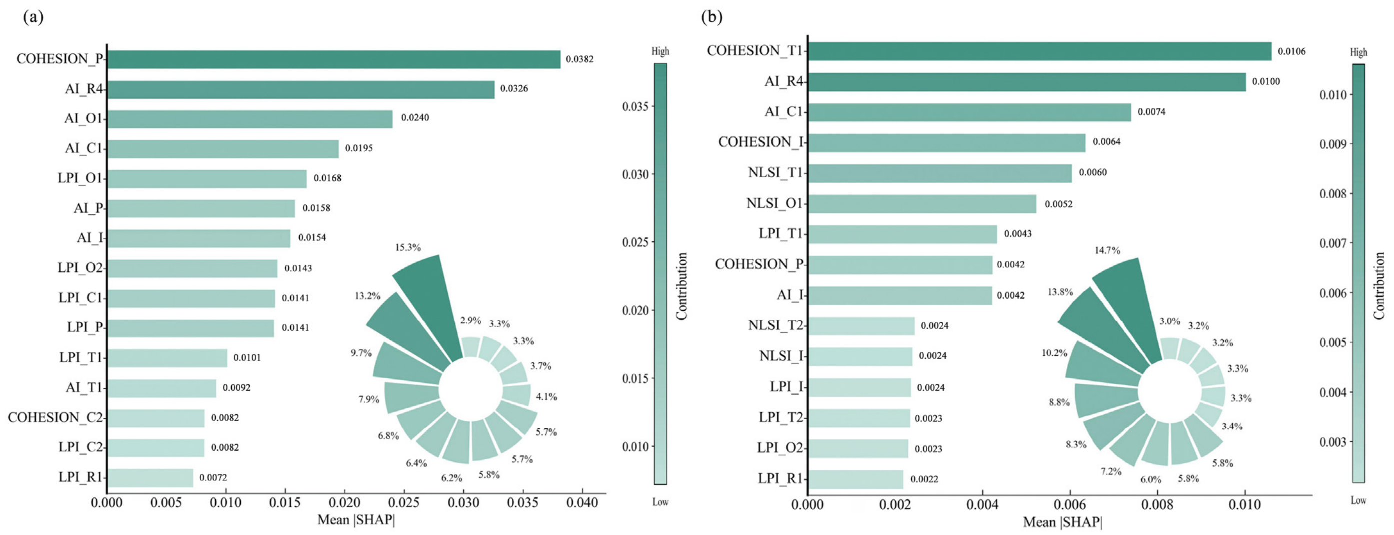

Figure 10. Differences in the contributions of morphology indicators to CEI between (**a**) core and (**b**) peripheral cities.

A comparison of SHAP summary plots for structure-related indicators (Figure 11) indicates that CEI in core cities is largely dominated by a small number of structural indicators, whereas in peripheral cities it is jointly shaped by gravitational interactions among multiple UFZs and land-use functional diversity. In core cities, the gravitational interactions between OZ and C1Z exhibit substantially higher importance than other structural indicators and play a dominant role in influencing CEI. In contrast, in peripheral cities, the contributions of gravitational interactions between OZ and other UFZs, as well as between RZ and other UFZs, increase markedly. At the same time, the influence of functional diversity also becomes more pronounced, jointly shaping CEI outcomes. These findings demonstrate that the structural mechanisms affecting CEI differ substantially across stages of urban development, further emphasizing that low-carbon-oriented urban structural optimization should explicitly account for city development stage and adopt functionally targeted regulation strategies accordingly.

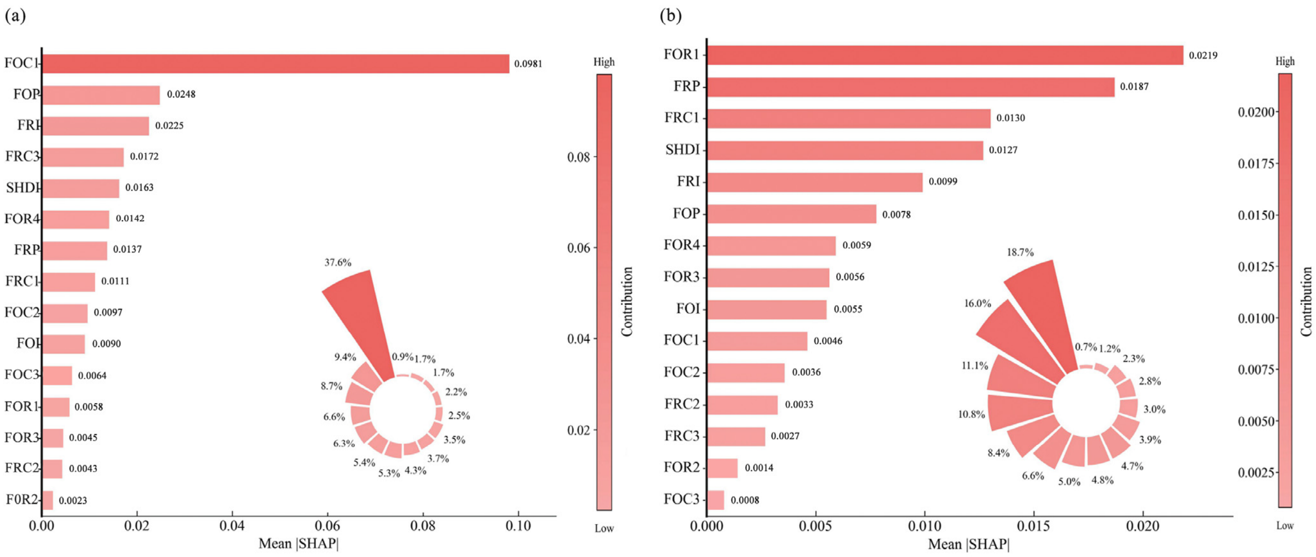

Figure 11. Differences in the contributions of structure indicators to CEI between (**a**) core and (**b**) peripheral cities.

5.4. Policy Implications

Urban zoning and development constitute the primary mechanisms guiding the spatial expansion and morphological evolution of cities. An unscientific configuration of UFZ may reduce the operational efficiency of individual UFZs, weaken inter-zonal coordination, and ultimately deteriorate overall environmental performance. Based on the identified driving mechanisms of carbon emission intensity, several policy-relevant implications can be derived.

(1) At the scale of the built-up urban area, priority should be given to regulating UFZ density. In particular, careful control over the proportions of green space, public service land, and residential land is essential to avoid carbon increases induced by excessive development intensity. Within this framework, a moderate expansion of plaza-type open spaces, together with improvements in transport infrastructure, can help alleviate excessive economic concentration and mitigate congestion along major transport corridors.

(2) At finer neighborhood or district scales, planning strategies should focus on the aggregation and connectivity of different functional land uses. Controlling the clustering intensity of residential and CZs, while simultaneously establishing well-structured transport networks, can enhance spatial connectivity and reduce carbon emissions associated with traffic congestion and inefficient mobility patterns.

(3) At larger subregional scales, inter-zonal relationships and land-use compositional diversity become increasingly important. Carbon emission intensity at this scale is par-

ticularly sensitive to the configuration of open spaces. Strengthening spatial linkages between open spaces, public service facilities, and low-density mid-rise residential areas can partially offset the negative environmental impacts of urban expansion. In addition, promoting land-use diversity within a reasonable range can enhance overall development quality and generate positive environmental effects, although the risks associated with excessive diversification should also be carefully managed.

(4) For core cities, carbon emission intensity is mainly driven by a limited number of key UFZ types and their spatial organization. Policy design should therefore emphasize refined and targeted regulation of critical land-use categories, focusing on improving the efficiency of green spaces, commercial areas, and public service land, as well as optimizing spatial coordination among major UFZs.

(5) In peripheral cities, carbon emission intensity is jointly shaped by multiple UFZs and their interactions. Policy interventions should prioritize the coordinated allocation of residential, green, public service, and transport land. Measures such as promoting jobs–housing balance, improving transport network structures, and controlling disorderly spatial expansion are crucial for reducing energy consumption associated with daily travel and production activities.

6. Conclusions

This study investigates the mechanisms through which UFZ form influences carbon emission intensity. By approaching low-carbon development from the perspective of UFZ form, it emphasizes the importance of scale sensitivity and nonlinear effects in shaping the relationship between urban morphology and CEI. Based on the research objectives outlined above, several key findings can be summarized as follows.

(1) The effects of UFZ form on CEI exhibit strong scale dependency. Based on the dimensional contribution ratios derived from the PCA results, the density dimension shows a pattern that remains relatively stable at smaller scales and then increases with scale expansion, whereas the morphology and structure dimensions display distinct U-shaped and inverted U-shaped relationships with spatial scale. Their explanatory power peaks at grid sizes of 14 km, 5 km, and 7 km, respectively, with contribution shares of 61.8 percent, 55.7 percent, and 74.4 percent at their optimal scales. The divergence in optimal scales across dimensions reflects a clear spatial transition from localized morphological effects to mid-scale functional configuration effects, and ultimately to large-scale land-use composition effects.

(2) UFZ with similar functional attributes and difference in building and green space configuration exert differentiated impacts on CEI. Within the density dimension, O1Z, PZ, and R2Z emerge as the most influential UFZ. In the morphology dimension, although identical indicators do not exhibit uniform effects across all UFZs, COHESION and AI consistently show the strongest explanatory power for CEI. In the structure dimension, F_{OX} generally exerts a stronger influence than F_{RX}. Overall, F_{OR1}, F_{RP}, and F_{OP} show particularly pronounced effects on carbon emissions, while SHDI also plays an important role.

(3) The impacts of UFZ form on CEI vary by zone type, with most indicators displaying nonlinear patterns and threshold-based sign reversals. Indicators such as PLAND, AI, and COHESION, as well as structural indicators including F_{OX}, F_{RX}, and SHDI, exhibit carbon mitigation effects within certain ranges. However, these effects are subject to diminishing marginal returns and may reverse into carbon-increasing impacts once critical thresholds are exceeded. This finding highlights the necessity of threshold-based and fine-grained regulation of UFZ form rather than uniform or monotonic control strategies.

Despite its contributions, this study has several limitations. First, although the functional zoning framework integrates multi-source data and achieves high classification accuracy, uncertainties remain due to incomplete POI data and the inherent ambiguity of mixed-use urban spaces. Second, while the multi-scale grid approach helps mitigate the MAUP, scale selection is inherently constrained by predefined grid increments. Alternative delineations based on administrative boundaries or urban functional cores may yield nuanced insights into morphological effects. Finally, although optimal scales are identified using cumulative variance contribution ratios, the dominance of a specific scale does not preclude the secondary influences of others, which may still affect local outcomes. Future research should address these gaps through more comprehensive scale definitions, refined functional zoning methods, and integrated multi-scale analytical frameworks.

Author Contributions: Conceptualization, W.X., M.W. and M.Z.; methodology, W.X. and M.W.; software, W.X. and M.W.; validation, W.X., M.W. and M.Z.; formal analysis, W.X.; investigation, W.X., M.W. and M.Z.; resources, W.X., M.Z. and J.L.; data curation, W.X. and M.W.; writing—original draft preparation, W.X.; writing—review and editing, M.Z. and J.L.; visualization, W.X.; supervision, M.Z. and J.L.; project administration, M.Z. and J.L. All authors have read and agreed to the published version of the manuscript.

Funding: This research received no external funding.

Institutional Review Board Statement: Not applicable.

Informed Consent Statement: Not applicable.

Data Availability Statement: The original contributions presented in this study are included in the article. Further inquiries can be directed to the corresponding author.

Acknowledgments: The authors gratefully acknowledge Northeast Forestry University and Tianjin University for their support.

Conflicts of Interest: The authors declare no conflicts of interest.

Abbreviations

The following abbreviations are used in this manuscript:

CEI	Carbon emission intensity
UFZ	Urban functional zone
MAPU	Modifiable areal unit problem
YRD	Yangtze River Delta
GDP	Gross Domestic Product
NDVI	Normalized Difference Vegetation Index
POI	Point of Interest
SHAP	Shapley additive explanations
PCA	Principal component analysis
UDI	Urban Development Intensity
RZ	Residential Zone
R1Z	High-density mid- and low-rise residential Zone
R2Z	Low-density mid- and high residential Zone
R3Z	High-density mid- and high residential zone
R4Z	Low-density mid- and low-rise residential zone
CZ	Commercial zone
C1Z	Other commercial zone
C2Z	Individual commercial zone
C3Z	High-level commercial zone
IZ	Industrial zone

PZ	Public zone
TZ	Transportation zone
T1Z	Transportation road zone
T2Z	Transportation facilities zone
OZ	Open space zone
O1Z	Open green space zone
O2Z	Open square space zone
PLAND	Percentage of landscape
NLSI	Normalized landscape shape index
AI	Aggregation index
LPI	Largest patch index
COHESION	Patch cohesion index
FCI	Functional compactness index
RFCI	Residential functional compactness index
OFCI	Open space functional compactness index
SHDI	Shannon's diversity index
VIF	Variance inflation factor
LOWESS	Locally weighted scatterplot smoothing

References

1. Tollefson, J. IPCC climate report: Earth is warmer than it's been in 125,000 years. *Nature* **2021**, *596*, 171–172. [CrossRef]
2. Hansen, J.; Lebedeff, S. Global trends of measured surface air temperature. *J. Geophys. Res.* **1987**, *92*, 13345–13372. [CrossRef]
3. Leisner, C.P. Review: Climate change impacts on food security- focus on perennial cropping systems and nutritional value. *Plant Sci.* **2020**, *293*, 110412. [CrossRef] [PubMed]
4. Pata, U.K. Renewable energy consumption, urbanization, financial development, income and CO_2 emissions in Turkey: Testing EKC hypothesis with structural breaks. *J. Clean. Prod.* **2018**, *187*, 770–779. [CrossRef]
5. Seto, K.C.; Fragkias, M.; Guneralp, B.; Reilly, M.K. A meta-analysis of global urban land expansion. *PLoS ONE* **2011**, *6*, e23777. [CrossRef] [PubMed]
6. Ouyang, X.; Lin, B. Carbon dioxide (CO_2) emissions during urbanization: A comparative study between China and Japan. *J. Clean. Prod.* **2017**, *143*, 356–368. [CrossRef]
7. Tian, Y.; Yin, K.; Lu, D.; Hua, L.; Zhao, Q.; Wen, M. Examining Land Use and Land Cover Spatiotemporal Change and Driving Forces in Beijing from 1978 to 2010. *Remote Sens.* **2014**, *6*, 10593–10611. [CrossRef]
8. Jia, X.; Zhang, Y.; Tan, R.R.; Li, Z.; Wang, S.; Wang, F.; Fang, K. Multi-objective energy planning for China's dual carbon goals. *Sustain. Prod. Consum.* **2022**, *34*, 552–564. [CrossRef]
9. Zhao, X.; Ma, X.; Chen, B.; Shang, Y.; Song, M. Challenges toward carbon neutrality in China: Strategies and countermeasures. *Resour. Conserv. Recycl.* **2022**, *176*, 105959. [CrossRef]
10. Ou, J.; Liu, X.; Li, X.; Chen, Y. Quantifying the relationship between urban forms and carbon emissions using panel data analysis. *Landsc. Ecol.* **2013**, *28*, 1889–1907. [CrossRef]
11. Qiliang, M.; Linlu, L.; Wenyan, J. Industrial policy and spatial arrangement of land leasing in China: A case of Jiangsu Province. *Cities* **2023**, *139*, 104401. [CrossRef]
12. Yang, Y.; Xie, B.; Lyu, J.; Liang, X.; Ding, D.; Zhong, Y.; Song, T.; Chen, Q.; Guan, Q. Optimizing urban functional land towards "dual carbon" target: A coupling structural and spatial scales approach. *Cities* **2024**, *148*, 104860. [CrossRef]
13. Jiang, Y.; Long, Y.; Liu, Q.; Dowaki, K.; Ihara, T. Carbon emission quantification and decarbonization policy exploration for the household sector—Evidence from 51 Japanese cities. *Energy Policy* **2020**, *140*, 111438. [CrossRef]
14. Sun, C.; Zhang, Y.; Ma, W.; Wu, R.; Wang, S. The Impacts of Urban Form on Carbon Emissions: A Comprehensive Review. *Land* **2022**, *11*, 1430. [CrossRef]
15. Shi, F.; Liao, X.; Shen, L.; Meng, C.; Lai, Y. Exploring the spatiotemporal impacts of urban form on CO2 emissions: Evidence and implications from 256 Chinese cities. *Environ. Impact Assess. Rev.* **2022**, *96*, 106850. [CrossRef]
16. Fang, C.; Wang, S.; Li, G. Changing urban forms and carbon dioxide emissions in China: A case study of 30 provincial capital cities. *Appl. Energy* **2015**, *158*, 519–531. [CrossRef]
17. Rahman, M.M.; Sultana, N.; Velayutham, E. Renewable energy, energy intensity and carbon reduction: Experience of large emerging economies. *Renew. Energy* **2022**, *184*, 252–265. [CrossRef]
18. Zhou, B.; Zhang, C.; Song, H.; Wang, Q. How does emission trading reduce China's carbon intensity? An exploration using a decomposition and difference-in-differences approach. *Sci. Total Environ.* **2019**, *676*, 514–523. [CrossRef] [PubMed]

19. Dong, F.; Hu, M.; Gao, Y.; Liu, Y.; Zhu, J.; Pan, Y. How does digital economy affect carbon emissions? Evidence from global 60 countries. *Sci. Total Environ.* **2022**, *852*, 158401. [CrossRef] [PubMed]
20. Ji, Q.; Li, C.; Makvandi, M.; Zhou, X. Impacts of urban form on integrated energy demands of buildings and transport at the community level: A comparison and analysis from an empirical study. *Sustain. Cities Soc.* **2022**, *79*, 103680. [CrossRef]
21. Mussawar, O.; Mayyas, A.; Azar, E. Built form and function as determinants of urban energy performance: An integrated agent-based modeling approach and case study. *Sustain. Cities Soc.* **2023**, *96*, 104660. [CrossRef]
22. Iungman, T.; Khomenko, S.; Barboza, E.P.; Cirach, M.; Goncalves, K.; Petrone, P.; Erbertseder, T.; Taubenbock, H.; Chakraborty, T.; Nieuwenhuijsen, M. The impact of urban configuration types on urban heat islands, air pollution, CO(2) emissions, and mortality in Europe: A data science approach. *Lancet Planet Health* **2024**, *8*, e489–e505. [CrossRef] [PubMed]
23. Shang, S.; Du, S.; Du, S.; Zhu, S. Estimating building-scale population using multi-source spatial data. *Cities* **2021**, *111*, 103002. [CrossRef]
24. Ma, X.; Yang, J.; Sun, D.; Zhang, R.; Xiao, X.; Xia, J. Fine allocation of sectoral carbon emissions at block scale and contribution of functional zones. *Ecol. Inform.* **2023**, *78*, 102293. [CrossRef]
25. Huang, Y.; Li, S.; Lin, J.; Zheng, L.; Zhuang, C.; Guan, C.; Guo, Y.; Zhuang, Y. Nonlinear and threshold effects of urban building form on carbon emissions. *Energy Build.* **2025**, *329*, 115243. [CrossRef]
26. Li, G.; Wang, W.; Li, B.; Duan, Z.; Hu, L.; Liu, J. Spatiotemporal simulation of blue-green space pattern evolution and carbon storage under different SSP-RCP scenarios in Wuhan. *Sci. Rep.* **2025**, *15*, 4017. [CrossRef] [PubMed]
27. Lan, T.; Shao, G.; Xu, Z.; Tang, L.; Dong, H. Considerable role of urban functional form in low-carbon city development. *J. Clean. Prod.* **2023**, *392*, 136256. [CrossRef]
28. Lee, D.; Robertson, C.; Ramsay, C.; Pyper, K. Quantifying the impact of the modifiable areal unit problem when estimating the health effects of air pollution. *Environmetrics* **2020**, *31*, e2643. [CrossRef]
29. Anderson, W.P.; Kanaroglou, P.S.; Miller, E.J. Urban Form, Energy and the Environment: A Review of Issues, Evidence and Policy. *Urban Stud.* **1996**, *33*, 7–35. [CrossRef]
30. Qi, J.; Xiong, W.; Li, J.; Zheng, J.; Ye, Q.; Hu, M. Investigating non-linear and synergistic effects of urban functional zone morphology on land surface temperature. *Sustain. Cities Soc.* **2025**, *130*, 106546. [CrossRef]
31. Xing, X.; Shi, W.; Wu, X.; Liu, Y.; Wang, X.; Zhang, Y. Towards a more compact urban form: A spatial-temporal study on the multi-dimensional compactness index of urban form in China. *Appl. Geogr.* **2024**, *171*, 103368. [CrossRef]
32. Murathan, E.K.; Manioğlu, G. Impact of urban form on energy performance, outdoor thermal comfort, and urban heat island: A case study in Istanbul. *Energy Build.* **2025**, *345*, 116109. [CrossRef]
33. Zhang, W.; Huang, B.; Luo, D. Effects of land use and transportation on carbon sources and carbon sinks: A case study in Shenzhen, China. *Landsc. Urban Plan.* **2014**, *122*, 175–185. [CrossRef]
34. Huo, T.; Li, X.; Cai, W.; Zuo, J.; Jia, F.; Wei, H. Exploring the impact of urbanization on urban building carbon emissions in China: Evidence from a provincial panel data model. *Sustain. Cities Soc.* **2020**, *56*, 102068. [CrossRef]
35. Liu, Z.; Xu, Q.; Lyu, S.; Yang, R.; Wan, Z. A Review of the Impact of Urban Form on Building Carbon Emissions. *Buildings* **2025**, *15*, 2604. [CrossRef]
36. Fleischmann, M.; Romice, O.; Porta, S. Measuring urban form: Overcoming terminological inconsistencies for a quantitative and comprehensive morphologic analysis of cities. *Environ. Plan. B Urban Anal. City Sci.* **2020**, *48*, 2133–2150. [CrossRef]
37. An, Y.; Wen, G.; Fan, M.; Zhao, P.; Sun, J.; He, M.; Bao, H.; Li, Y.; Li, N.; Zhang, F.; et al. Towards sustainable urban development: Decoding the spatiotemporal relationship between urban spatial structure and carbon emissions. *Carbon Balance Manag.* **2025**, *20*, 17. [CrossRef] [PubMed]
38. Feng, T.; Zhou, B. Impact of urban spatial structure elements on carbon emissions efficiency in growing megacities: The case of Chengdu. *Sci. Rep.* **2023**, *13*, 9939. [CrossRef] [PubMed]
39. Hong, S.; Hui, E.C.-m.; Lin, Y. Relationship between urban spatial structure and carbon emissions: A literature review. *Ecol. Indic.* **2022**, *144*, 109456. [CrossRef]
40. Wu, J.; Jones, K.B.; Li, H.; Loucks, O.L. *Concepts of Scale and Scaling*; Springer: Dordrecht, The Netherlands, 2006; pp. 3–15.
41. Moran, P.A.P. Notes on Continuous Stochastic Phenomena. *Biometrika* **1950**, *37*, 17–23. [CrossRef] [PubMed]
42. Tan, G.; Zhang, X.; Xiong, S.; Sun, Z.; Lei, Y.; Wang, H.; Du, S. Assessing the impacts of urban functional form on anthropogenic carbon emissions: A case study of 31 major cities in China. *Ecol. Indic.* **2024**, *167*, 112700. [CrossRef]
43. Huang, X.; Wang, Y. Investigating the effects of 3D urban morphology on the surface urban heat island effect in urban functional zones by using high-resolution remote sensing data: A case study of Wuhan, Central China. *ISPRS J. Photogramm. Remote Sens.* **2019**, *152*, 119–131. [CrossRef]
44. Liu, Y.; Zhang, W.; Liu, W.; Tan, Z.; Hu, S.; Ao, Z.; Li, J.; Xing, H. Exploring the seasonal effects of urban morphology on land surface temperature in urban functional zones. *Sustain. Cities Soc.* **2024**, *103*, 105268. [CrossRef]
45. Tu, Y.; Chen, B.; Zhang, T.; Xu, B. Regional Mapping of Essential Urban Land Use Categories in China: A Segmentation-Based Approach. *Remote Sens.* **2020**, *12*, 1058. [CrossRef]

46. Liu, H.; Huang, B.; Zhan, Q.; Gao, S.; Li, R.; Fan, Z. The influence of urban form on surface urban heat island and its planning implications: Evidence from 1288 urban clusters in China. *Sustain. Cities Soc.* **2021**, *71*, 102987. [CrossRef]
47. Chen, Y.; Huang, L. Modeling growth curve of fractal dimension of urban form of Beijing. *Phys. A Stat. Mech. Its Appl.* **2019**, *523*, 1038–1056. [CrossRef]
48. Qiao, J.; Li, Y.; Yu, J. Administrative-led urbanization and urban carbon emission intensity: Evidence from city-county merger in China. *Energy Econ.* **2024**, *136*, 107615. [CrossRef]
49. Lan, T.; Shao, G.; Xu, Z.; Tang, L.; Sun, L. Measuring urban compactness based on functional characterization and human activity intensity by integrating multiple geospatial data sources. *Ecol. Indic.* **2021**, *121*, 107177. [CrossRef]
50. Zhang, Y.; Wang, Y.; Ding, N.; Yang, X. Spatial Pattern Impact of Impervious Surface Density on Urban Heat Island Effect: A Case Study in Xuzhou, China. *Land* **2022**, *11*, 2135. [CrossRef]
51. Chertow, M.R. The IPAT Equation and Its Variants. *J. Ind. Ecol.* **2000**, *4*, 13–29. [CrossRef]
52. Chen, T.; Guestrin, C. XGBoost: A Scalable Tree Boosting System. In *Proceedings of the 22nd ACM SIGKDD International Conference on Knowledge Discovery and Data Mining, San Francisco, CA, USA, 13–17 August 2016*; Association for Computing Machinery: New York, NY, USA, 2016; pp. 785–794. [CrossRef]
53. Xu, C.; Xiong, W.; Zhang, S.; Shi, H.; Wu, S.; Bao, S.; Xiao, T. Research on the Nonlinear Relationship Between Carbon Emissions from Residential Land and the Built Environment: A Case Study of Susong County, Anhui Province Using the XGBoost-SHAP Model. *Land* **2025**, *14*, 440. [CrossRef]
54. Shlens, J. A Tutorial on Principal Component Analysis. *Int. J. Remote Sens.* **2014**, *51*.
55. Zaki, A.; Przewoźna, P.; Matczak, P.; Witkowski, M.; Kuchcik, M.; Jabkowski, P. Principal component analysis and fuzzy clustering for neighborhood-scale urban morphology-based thermal hazard assessment. *Sustain. Cities Soc.* **2026**, *147*, 107551. [CrossRef]
56. Han, D.; An, H.; Wang, F.; Xu, X.; Qiao, Z.; Wang, M.; Sui, X.; Liang, S.; Hou, X.; Cai, H.; et al. Understanding seasonal contributions of urban morphology to thermal environment based on boosted regression tree approach. *Build. Environ.* **2022**, *226*, 109770. [CrossRef]
57. Davtalab, M.; Byčenkienė, S. Synergistic effects of spatial urban form on PM2.5 concentration and urban heat islands: A multi-scale explanatory machine learning. *J. Clean. Prod.* **2026**, *538*, 147226. [CrossRef]
58. Li, Y.; Zhang, Y.; Wu, Q.; Xue, R.; Wang, X.; Si, M.; Zhang, Y. Greening the concrete jungle: Unveiling the co-mitigation of greenspace configuration on PM2.5 and land surface temperature with explanatory machine learning. *Urban For. Urban Green.* **2023**, *88*, 128086. [CrossRef]
59. Meng, J.; Han, W.; Yuan, C. Seasonal and multi-scale difference of the relationship between built-up land landscape pattern and PM2.5 concentration distribution in Nanjing. *Ecol. Indic.* **2023**, *156*, 111079. [CrossRef]
60. Li, S.; Sun, Z.; Wen, R.; Yang, H.; Li, J.; Chen, T.; Zheng, Y.; Zhu, N. Spatiotemporal patterns and the influence mechanism of urban landscape pattern on carbon emission performance: Evidence from Chinese cities. *Sustain. Cities Soc.* **2025**, *118*, 106042. [CrossRef]
61. Wang, S.; Zeng, X.; Huang, Y.; Li, X. Analysing urban local cold air dynamics and climate functional zones using interpretable machine learning: A case study of Tianhe district, Guangzhou. *Sustain. Cities Soc.* **2024**, *114*, 105731. [CrossRef]
62. Wang, X.; Li, Z.; Kee, T. Spatial and temporal correlation between green space landscape pattern and carbon emission—Three major coastal urban agglomerations in China. *Urban Clim.* **2024**, *58*, 102222. [CrossRef]
63. Belgiu, M.; Drăguţ, L. Random forest in remote sensing: A review of applications and future directions. *ISPRS J. Photogramm. Remote Sens.* **2016**, *114*, 24–31. [CrossRef]
64. Zhang, J.; Cui, P.; Song, H. Impact of urban morphology on outdoor air temperature and microclimate optimization strategy base on Pareto optimality in Northeast China. *Build. Environ.* **2020**, *180*, 107035. [CrossRef]
65. Boeing, G.; Pilgram, C.; Lu, Y. Urban street network design and transport-related greenhouse gas emissions around the world. *Transp. Res. Part D Transp. Environ.* **2024**, *127*, 103961. [CrossRef]
66. Liu, Y.; Wu, Y.; Zhu, X. Industrial clusters and carbon emission reduction: Evidence from China. *Ann. Reg. Sci.* **2024**, *73*, 557–597. [CrossRef]
67. Tang, H.; Qiu, H.; Yang, Y. Thermal environment disparities across 11 cities in the greater bay area: Nonlinear relationships and urban greening-based solutions. *Sustain. Cities Soc.* **2025**, *133*, 106867. [CrossRef]
68. Zhang, S.; Ding, J.; Zheng, H.; Wang, H. Does spatial functional division in urban agglomerations reduce negative externalities in large cities? Evidence from urban agglomerations in China. *Heliyon* **2023**, *9*, e20419. [CrossRef] [PubMed]
69. Zhang, S.; Miao, X.; Zheng, H.; Chen, W.; Wang, H. Spatial functional division in urban agglomerations and carbon emission intensity: New evidence from 19 urban agglomerations in China. *Energy* **2024**, *300*, 131541. [CrossRef]